Article

CRISPR activation for *SCN2A*-related neurodevelopmental disorders

https://doi.org/10.1038/s41586-025-09522-w

Received: 23 January 2024

Accepted: 13 August 2025

Published online: 17 September 2025

Check for updates

Serena Tamura[1,2,11], Andrew D. Nelson[3,4,11], Perry W. E. Spratt[3,4,11], Elizabeth C. Hamada[3,4], Xujia Zhou[1,2], Henry Kyoung[3,4], Zizheng Li[1,2], Coline Arnould[1,2], Vladyslav Barskyi[1,2], Beniamin Krupkin[1,2], Kiana Young[1,2], Jingjing Zhao[1,2], Stephanie S. Holden[4,5], Atehsa Sahagun[3,4], Caroline M. Keeshen[3,4], Congyi Lu[6], Roy Ben-Shalom[3,4], Sunrae E. Taloma[3,4], Selin Schamiloglu[3,4], Ying C. Li[3,4], Lia Min[7], Paul M. Jenkins[7,8], Jen Q. Pan[6], Jeanne T. Paz[4,5], Stephan J. Sanders[3,9,10], Navneet Matharu[1,2], Nadav Ahituv[1,2]✉ & Kevin J. Bender[3,4]✉

Most neurodevelopmental disorders with single gene diagnoses act via haploinsufficiency, in which only one of the two gene copies is functional[1]. *SCN2A* haploinsufficiency is one of the most frequent causes of neurodevelopmental disorder, often presenting with autism spectrum disorder, intellectual disability and, in a subset of children, refractory epilepsy[2]. Here, using *SCN2A* haploinsufficiency as a proof-of-concept, we show that upregulation of the existing functional gene copy through CRISPR activation (CRISPRa) can rescue neurological-associated phenotypes in *Scn2a* haploinsufficient mice. We first show that restoring *Scn2a* expression in adolescent heterozygous *Scn2a* conditional knock-in mice rescues electrophysiological deficits associated with *Scn2a* haploinsufficiency (*Scn2a*$^{+/-}$). Next, using an adeno-associated virus CRISPRa-based treatment in adolescent mice, we show that we can correct intrinsic and synaptic deficits in neocortical pyramidal cells, a major cell type that contributes to neurodevelopmental disorders and seizure aetiology in *SCN2A* haploinsufficiency. Furthermore, we find that systemic delivery of CRISPRa protects *Scn2a*$^{+/-}$ mice against chemoconvulsant-induced seizures. Finally, we also show that adeno-associated virus CRISPRa treatment rescues excitability in *SCN2A* haploinsufficient human stem-cell-derived neurons. Our results showcase the potential of this therapeutic approach to rescue *SCN2A* haploinsufficiency and demonstrates that rescue even at adolescent stages can ameliorate neurodevelopmental phenotypes.

Neurodevelopmental disorders (NDDs), including intellectual disability, autism spectrum disorder (ASD) and early-onset epilepsy, affect over 3% of the general population in the USA[3]. Recent advances in gene discovery have facilitated the identification of 387 high-confidence genes associated with NDDs from autosomal germline de novo variants[4–6]. Altogether, 227 of these NDD genes are either known or predicted to cause ASD due to haploinsufficiency, in which the messenger RNA/protein levels from the residual gene copy are insufficient to enable the typical function of the gene[1]. Gene replacement therapy could potentially restore transcriptional balance and rectify deficits in haploinsufficient diseases by delivering functional gene copies. However, in most NDD-related genes, traditional gene therapy vectors cannot be used. Gene therapy relies primarily on using recombinant adeno-associated virus (rAAV) for transgene delivery owing to the limited pathogenicity and long-term transgene expression of the virus[7]. However, rAAV has a limited packaging capacity (4,700-base pair (bp) optimal packaging capacity minus about 1,700 bp needed for transgene expression)[8]. Examination of the coding sequence length of the 227 haploinsufficient NDD-associated genes shows that 117 exceed rAAV vector capacity (Supplementary Table 1), excluding them from traditional gene replacement therapy approaches[9].

Here we tested whether *cis*-regulation therapy (CRT) could be a viable approach for treating NDD-associated haploinsufficiency. CRT uses a nuclease-deficient gene-editing system, such as a 'dead' Cas9 (dCas9), fused to a transcriptional modulator to target gene regulatory elements (such as promoters or enhancers) and alter gene expression[10]. For this study, we used dCas9 fused to a transcriptional activator, termed CRISPR activation (CRISPRa), to upregulate gene expression and correct haploinsufficiency by targeting a gene promoter. For our proof-of-concept, we used NDD-associated haploinsufficiency of the sodium voltage-gated channel alpha subunit 2 (*SCN2A*), a gene with a 6-kilobase (kb)-long coding sequence[9]. Variants in this gene can

[1]Department of Bioengineering and Therapeutic Sciences, University of California San Francisco, San Francisco, CA, USA. [2]Institute for Human Genetics, University of California San Francisco, San Francisco, CA, USA. [3]Weill Institute for Neurosciences, University of California San Francisco, San Francisco, CA, USA. [4]Department of Neurology, University of California San Francisco, San Francisco, CA, USA. [5]Gladstone Institute of Neurological Disease, University of California San Francisco, San Francisco, CA, USA. [6]Stanley Center for Psychiatric Research, Broad Institute, Cambridge, MA, USA. [7]Department of Pharmacology, University of Michigan Medical School, Ann Arbor, MI, USA. [8]Department of Psychiatry, University of Michigan Medical School, Ann Arbor, MI, USA. [9]Department of Psychiatry, University of California San Francisco, San Francisco, CA, USA. [10]Institute of Developmental and Regenerative Medicine, Department of Paediatrics, University of Oxford, Oxford, UK. [11]These authors contributed equally: Serena Tamura, Andrew D. Nelson, Perry W. E. Spratt. ✉e-mail: nadav.ahituv@ucsf.edu; kevin.bender@ucsf.edu

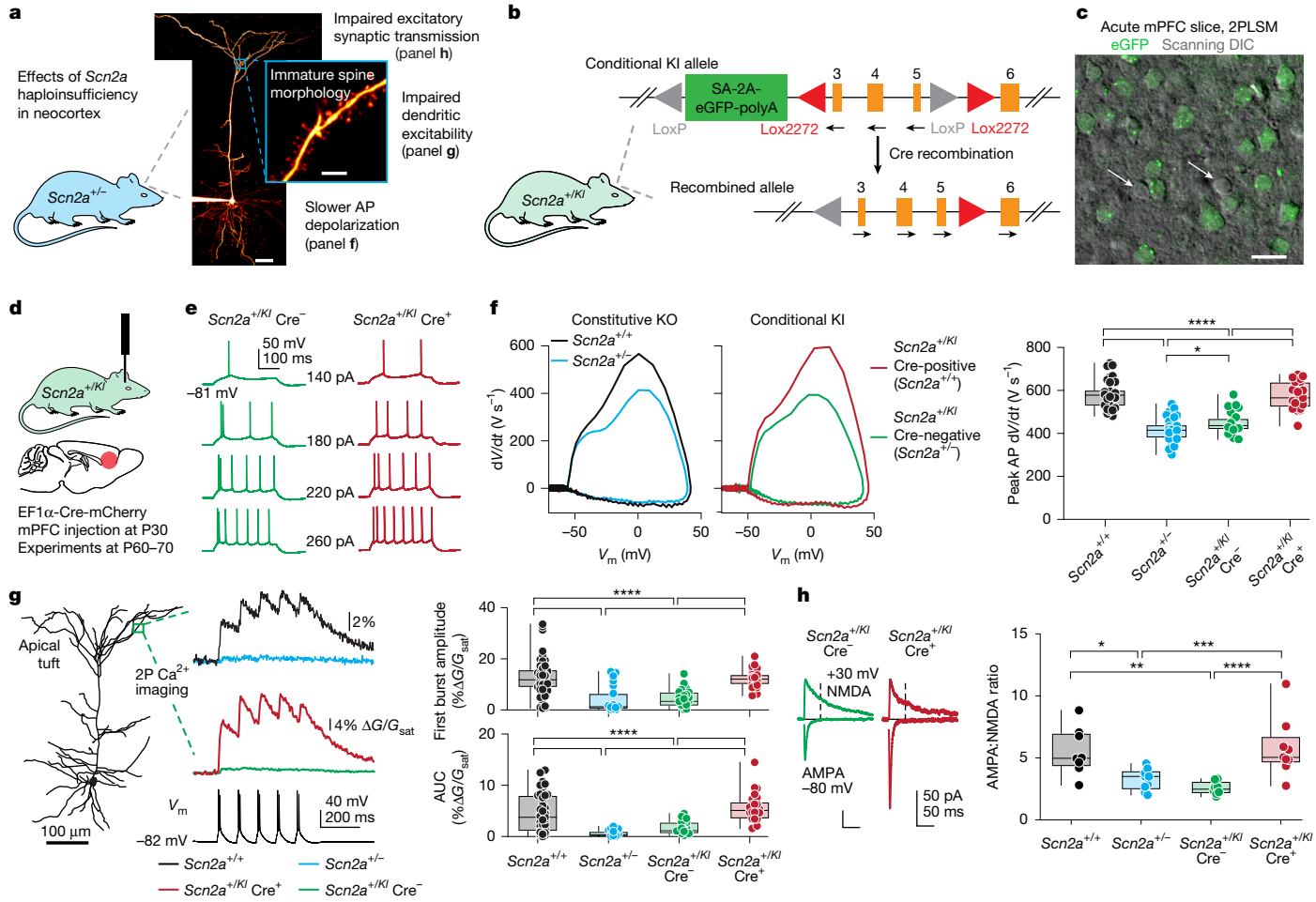

Fig. 1 | Genetic rescue of *Scn2a* haploinsufficiency in adolescent mice rescues electrophysiological deficits. a, Summary of *Scn2a* haploinsufficiency effects on mouse mPFC layer 5b pyramidal neurons (L5PNs). **b**, Strategy for genetic restoration of *Scn2a* in *Scn2a*$^{+/KI}$ conditional knock-in model. **c**, 2PLSM *z*-stack of layer 5 mPFC in acute slice from *Scn2a*$^{+/KI}$ mouse without Cre injection. Arrows highlight GFP-negative, presumptive interneurons. **d**, Schematic of rAAV-EF1α-Cre-mCherry injection into the mPFC of P30 *Scn2a*$^{+/KI}$ mice. Electrophysiological and imaging experiments in *Scn2a*$^{+/KI}$ and control mice were performed between P60 and P70. **e**, APs per 300-ms stimulation epoch across a range of current amplitudes in *Scn2a*$^{+/KI}$ Cre-negative (green) and *Scn2a*$^{+/KI}$ Cre-positive (red) L5PNs. **f**, Left, representative phase-plane plots (d*V*/d*t* versus voltage) of somatic APs across conditions. Right, peak d*V*/d*t* of the first AP evoked by a near-rheobase current. $n = 44$ *Scn2a*$^{+/+}$, 37 *Scn2a*$^{+/-}$, 30 *Scn2a*$^{+/KI}$ Cre$^-$, 21 *Scn2a*$^{+/KI}$ Cre$^+$ cells. ****$P < 0.0001$, *$P = 0.02$, Holm–Šídák multiple comparisons test. **g**, Left, 2PLSM imaging of bAP-evoked Ca transients (doublet bursts) in L5PN apical dendrites (more than 400 µm from soma) across conditions. Right, Ca transient amplitude of the first of five bursts (top) and area under the curve (AUC) (bottom). $n = 49$ *Scn2a*$^{+/+}$, 23 *Scn2a*$^{+/-}$, 29 *Scn2a*$^{+/KI}$ Cre$^-$, 26 *Scn2a*$^{+/KI}$ Cre$^+$ imaging sites across ≥7 L5PNs per condition from ≥2 animals. ****$P < 0.0001$, Holm–Šídák multiple comparisons test. **h**, Left, AMPA and mixed AMPA/NMDA receptor-mediated EPSCs at –80 and +30 mV, respectively. NMDA receptor-mediated component measured 50 ms after stimulation (dotted line). Right, quantification of AMPA:NMDA ratio. $n = 8$ *Scn2a*$^{+/+}$, 9 *Scn2a*$^{+/-}$, 8 *Scn2a*$^{+/KI}$ Cre$^-$, 9 *Scn2a*$^{+/KI}$ Cre$^+$ cells. *$P = 0.02$, **$P = 0.004$, ***$P = 0.009$, ****$P = 0.002$, Holm–Šídák multiple comparisons test. Circles are single cells (**f**,**h**) or single imaging sites (**g**); box plots are medians, quartiles and 100% tails. Scale bars, 50 µm (**a**), 5 µm (**a**, inset), 20 µm (**c**). bAP, backpropagating action potential; %ΔG/G_{sat}, per cent change in green fluorescence, calibrated to maximal change; KI, knockin; KO, knockout; 2P, 2-photon.

enhance channel function, resulting in neonatal-onset seizure phenotypes, or inhibit channel function, resulting in *SCN2A*-related NDDs[2]. Loss-of-function (LoF) variants in *SCN2A* are one of the most prevalent genetically defined subsets of NDD, with an estimated incidence of around 300 births per year in the USA (about 1 in 12,000 births)[5]. *SCN2A*-related NDDs are characterized by severe intellectual disability, global developmental delay, ASD and seizures that can be refractory to traditional treatment methods[2].

SCN2A encodes the neuronal voltage-gated sodium channel, $Na_V1.2$, which is broadly expressed in the central nervous system (CNS), including in neocortical excitatory pyramidal cells whose dysfunction is implicated in NDD aetiology[11]. In the first year of life in humans and before postnatal day (P) 7 in mice, $Na_V1.2$ has an essential role as the primary Na_V responsible for action potential (AP) initiation in pyramidal cell axons[12]. After this period, $Na_V1.2$ is enriched throughout the somatic and dendritic domains in addition to the most proximal region of the axon initial segment (AIS)[13]. *Scn2a* haploinsufficiency in mice—either from birth (constitutive) or conditionally induced after P7—results in impairments in dendritic intrinsic excitability and excitatory synapse function[13,14] (Fig. 1a). This suggests that $Na_V1.2$ actively helps to maintain dendritic function throughout life and raises the possibility that rescue from *Scn2a* haploinsufficiency can be therapeutic, even if such a rescue is administered later in life.

As the intrinsic and synaptic deficits of *SCN2A* haploinsufficiency can be readily measured by means of electrophysiology, we hypothesized that *SCN2A* could provide an efficient and quantifiable model for CRT-based interventions. We administered rAAV-based CRISPRa targeting the *Scn2a* promoter to *Scn2a* heterozygous null mice and neurons differentiated from human embryonic stem cells (hESCs)[15] and demonstrate that this approach can rescue excitability deficits

in both models. In mice, we also observed that CRISPRa can rescue these deficits at adolescent stages and protect *Scn2a* heterozygous mice against chemoconvulsant-induced seizures. Combined, our work showcases a potential therapeutic approach that could be applied to many genes that, when haploinsufficient, are associated with NDDs and suggests that rescue later in life could ameliorate electrophysiological phenotypes associated with *Scn2a* haploinsufficiency.

Adolescent *Scn2a* rescue is therapeutic

To test the feasibility of increasing functional gene copy number to rescue the electrophysiological deficits associated with *Scn2a* haploinsufficiency, we first developed a conditional knock-in mouse line. In this mouse, termed *Scn2a*$^{+/KI}$, exons 3–5 of one *Scn2a* allele were flipped and flanked by LoxP sites, with an eGFP sequence in frame to visualize cells that express *Scn2a* (Fig. 1b). Acute slices were made from these animals, and neurons were visualized with two-photon laser scanning microscopy (2PLSM) of GFP fluorescence against a background image of neuropil imaged with 2PSLM scanning differential interference contrast (DIC) imaging (Fig. 1c). GFP-positive neurons targeted for whole-cell recordings had electrophysiological features indicative of *Scn2a*$^{+/-}$ pyramidal cells, including a decrease in the peak change in voltage during AP depolarization (peak dV/dt) relative to *Scn2a*$^{+/+}$ controls (Fig. 1c–f). Moreover, parvalbumin-positive interneurons were GFP-negative, consistent with known $Na_V1.2$ functional expression patterns[13,16] (Extended Data Fig. 1).

Previously, we showed that inducing *Scn2a* haploinsufficiency during adolescence impairs intrinsic and synaptic function[14]. To test whether these deficits can be rescued by gene reinstatement during adolescence, we injected rAAV-EF1α-Cre-mCherry into the medial prefrontal cortex (mPFC) of these *Scn2a*$^{+/KI}$ mice around P30 (Fig. 1d). After at least 4 weeks, to allow for transgene expression, mCherry-positive neurons were targeted for whole-cell recordings in acute slices. In the presence of Cre, several measures of neuronal and synaptic function were comparable to those found in wild-type (WT) mice, including peak AP dV/dt, AP-burst-evoked calcium influx in the apical dendritic tuft and AMPA:NMDA ratio, which is a common proxy for synapse strength and is abnormally low in *Scn2a*$^{+/-}$ cells[13] (Fig. 1f–h). Together, these data show that features of intrinsic and synaptic function that depend directly and indirectly on proper $Na_V1.2$ function can be restored to WT levels upon reactivation of the second allele in adolescent stages. They also suggest that the development of a CRT approach to increase the expression of the functional *SCN2A* allele could rescue deficits caused by haploinsufficiency.

Scn2a-CRISPRa optimization in vitro

To optimize an rAAV-based CRISPRa approach to rescue *Scn2a* haploinsufficiency, nine different single-guide RNAs (sgRNAs) targeting the *Scn2a* promoter were screened for their ability to upregulate *Scn2a* in mouse neuroblastoma cells (Neuro-2a). Guides were co-transfected with a *Staphylococcus aureus* (sa) dCas9 fused to the transcriptional activator VP64 (Supplementary Table 2). sadCas9-VP64 is compact in size (3.3 kb), allowing it to fit into an rAAV vector, and has been shown to promote upregulation to therapeutic levels in other forms of haploinsufficiency[17]. Three sgRNAs increased *Scn2a* mRNA levels and were packaged into an rAAV-DJ serotype vector, which provides high expression levels in many cell types and tissues, including neurons[18]. rAAV-sgRNA viruses were then co-transduced with the rAAV-sadCas9-VP64 activator, both using the adeno-associated virus (AAV)-DJ serotype, into Neuro-2a cells for 5 days. One of the three rAAV-sgRNAs was found to increase *Scn2a* mRNA expression by twofold and was selected for subsequent mouse studies (Extended Data Fig. 2a,b).

To test for off-target effects, we carried out RNA sequencing (RNA-seq) using two biological replicates and three technical replicates for each condition (six samples per condition) and analysed the mRNA expression of all genes in the same topologically associated domain (TAD) and all *Scn* sodium channel genes following plasmid CRISPRa transfection into Neuro-2a cells. We observed that *Scn2a* was the only upregulated gene in its TAD and also the only upregulated *Scn* sodium channel compared with negative control using RNA-seq (Extended Data Fig. 3a–c). We observed more genes to be upregulated compared with the negative control, with gene ontology (GO) analysis showing an enrichment for viral response (Extended Data Fig. 3d,e), probably from our AAV infection. In addition, we analysed differentially expressed genes that are close to (10 kb) sgRNA sequence off-targets using Cas-OFFinder[19] with sequences up to three mismatches and two bulges. With these criteria, we found six differentially expressed genes from our RNA-seq (Extended Data Fig. 3f). These include *Ptpn14* and one transcript with unknown function (*ENSMUSG00000125254*) which have a sequence hit with three mismatches and one bulge near the gene. We also found three genes (*Zfp697*, *Ifi44l* and *Csmd1*) and one transcript (*Gm17131*) with unknown function that have three mismatches and two bulges. Thus, the odds of the *Scn2a*-targeted sgRNA binding are low. Furthermore, *Ptpn14* regulates cell proliferation and is not known to have a major functional role in the brain[20]. The three other genes are related to viral response: *Zfp697* is involved in the mediation of interferon-γ response in muscle cells[21], *Ifi44l* is interferon-induced and involved in anti-viral response[22] and *Csmd1* is a complement inhibitor[23] that was downregulated. In summary, our results show that *Scn2a* is significantly upregulated with minimal off-target effects using our CRISPRa approach.

Cell-autonomous CRT in *Scn2a*$^{+/-}$ mice

To test whether *Scn2a*-rAAV-CRISPRa (rAAV-sadCas9-VP64 + rAAV-*Scn2a*-sgRNA) could be used as a therapeutic intervention for *Scn2a* haploinsufficiency in adolescent mice, we stereotaxically injected *Scn2a*-rAAV-CRISPRa into the mPFC of constitutive *Scn2a*$^{+/-}$ mice at about P30 (Supplementary Table 3). Mice were injected unilaterally in one hemisphere and the opposite hemisphere was used as a biologically matched uninjected control (Fig. 2a,b). As a negative (no sgRNA) control, *Scn2a*$^{+/-}$ mice were co-injected with rAAV-sadCas9-VP64 along with an rAAV-mCherry (termed empty vector). At least 4 weeks after injection, the mPFCs of the injected and uninjected hemispheres were dissected and extracted for quantitative PCR (qPCR) analysis and electrophysiological recordings. *Scn2a*$^{+/-}$ mice injected with *Scn2a*-rAAV-CRISPRa showed an upregulation of *Scn2a* mRNA of around 1.5-fold by means of reverse transcription quantitative PCR(RT–qPCR) compared with the uninjected hemisphere, whereas rAAV-empty-mCherry-injected mice showed no upregulation of *Scn2a* mRNA expression (Fig. 2c).

To assess the phenotypic effects of *Scn2a*-rAAV-CRISPRa on neuronal excitability, acute slices from the mPFC were dissected 4 weeks after injection and electrophysiological recordings were carried out from neurons in these slices. AP waveforms, measured with somatic current-clamp recordings, are sensitive to *Scn2a* expression levels in single cells, with peak dV/dt being directly proportional to $Na_V1.2$ density at the somatic membrane[13,24]. We found that peak dV/dt was restored to WT levels in mCherry-positive neurons in CRISPRa-treated *Scn2a*$^{+/-}$ mice (Fig. 2d). mCherry-negative neurons, recorded either from the same slices or in interleaved constitutive controls, showed dV/dt values expected for *Scn2a*$^{+/+}$ and *Scn2a*$^{+/-}$ neurons, respectively. Similarly, no upregulation in dV/dt was noted in mCherry-positive empty vector controls (Fig. 2d). Other aspects of neuronal excitability were stable (Extended Data Fig. 4).

Scn2a haploinsufficiency is also known to impair dendritic excitability and excitatory synapse function. We found that P30 *Scn2a*-rAAV-CRISPRa administration was able to rescue these impairments. AMPA:NMDA ratio was rescued to WT levels (Fig. 2e). Similarly, AP-evoked calcium transients in distal apical dendrites, which are

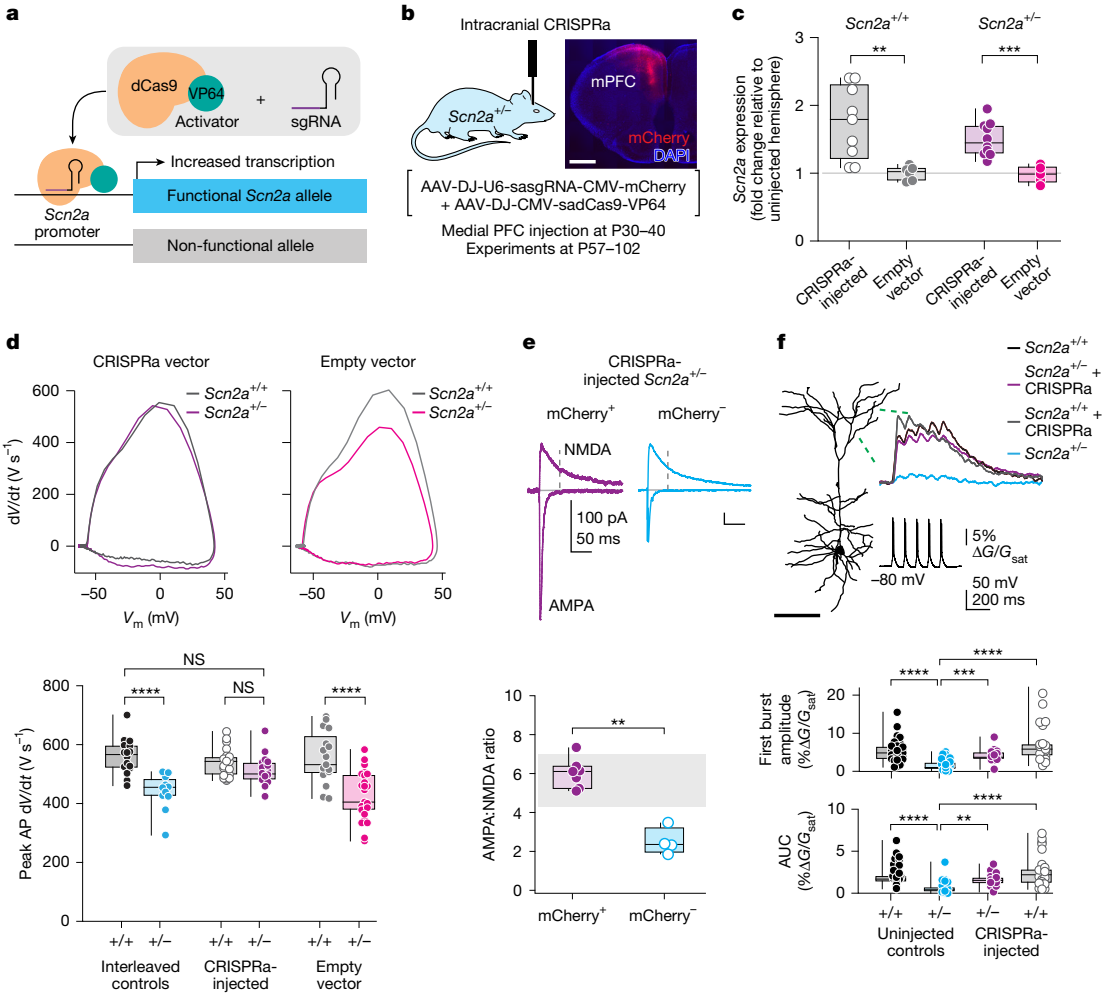

Fig. 2 | Intracranial *Scn2a*-rAAV-CRISPRa in mPFC rescues excitability deficits in *Scn2a*$^{+/-}$ neurons. a, CRT design to rescue *Scn2a* haploinsufficiency. **b**, Local injection of *Scn2a*-rAAV-CRISPRa (viruses injected in brackets) and coronal section detailing injection site, stained for mCherry and DAPI. **c**, RT–qPCR of *Scn2a* mRNA across conditions. $n = 9$ *Scn2a*$^{+/+}$ + CRISPRa, 6 *Scn2a*$^{+/+}$ + empty, 10 *Scn2a*$^{+/-}$ + CRISPRa, 5 *Scn2a*$^{+/-}$ + empty: 1.0 ± 0.06, $n = 5$ mice. $^{**}P = 0.0016$, $^{***}P = 0.0007$, Mann–Whitney test. **d**, AP phase-plane plots of CRT-treated and empty-treated *Scn2a*$^{+/+}$ and *Scn2a*$^{+/-}$ mice. Populations also compared with interleaved, uninjected controls. $n = 16$ *Scn2a*$^{+/+}$, 12 *Scn2a*$^{+/-}$, 24 *Scn2a*$^{+/+}$ + CRISPRa, 19 *Scn2a*$^{+/-}$ + CRISPRa, 17 *Scn2a*$^{+/+}$ + empty and 27 *Scn2a*$^{+/-}$ + empty cells. $^{****}P < 0.0001$, Holm–Šídák multiple comparisons test. **e**, AMPA:NMDA ratio, as in Fig. 1h, for *Scn2a*$^{+/-}$ + CRISPRa (mCherry^{+}, purple, $n = 7$) and *Scn2a*$^{+/-}$ (mCherry^{-}, cyan, $n = 4$) internal controls. Grey bar: 95% confidence interval of *Scn2a*$^{+/+}$ control data from ref. 13. $^{**}P = 0.006$, Mann–Whitney Wilcoxon test. **f**, bAP-evoked Ca imaging, as in Fig. 1g, in L5PNs from P55 to P84 *Scn2a*$^{+/+}$ (black, $n = 38$ sites, 11 cells, 5 mice), *Scn2a*$^{+/-}$ (cyan, $n = 40$ sites, 11 cells, 5 mice), *Scn2a*$^{+/-}$ + CRISPRa (purple, $n = 18$ sites, 5 cells, 5 mice) and *Scn2a*$^{+/+}$ + CRISPRa (grey, $n = 29$ sites, 8 cells, 8 mice). $^{**}P = 0.0002$, $^{***}P = 0.0004$, $^{****}P < 0.0001$, mixed-effect model, Holm–Šídák multiple comparisons test. Circles are animals (**c**), single cells (**d**,**e**) or imaging sites (**f**); box plots are medians, quartiles and 100% tails. Scale bars, 1 mm (b), 100 µm (**f**). NS, not significant.

readily observed in WT but not *Scn2a*$^{+/-}$ cells, were also restored (Fig. 2f). This suggests that CRT may be effective for *Scn2a* to help to re-engage such processes in the mPFC.

Systemic CRT in *Scn2a*$^{+/-}$ mice

We next explored the feasibility of intravenous systemic rAAV-CRISPRa delivery, as it is a more clinically translatable delivery approach. *Scn2a*$^{+/-}$ mice were injected, either through the tail vein or the retro-orbital sinus, with *Scn2a*-rAAV-CRISPRa constructs (sadCas9-VP64 and *Scn2a*-sgRNA) packaged using the PHP.eB rAAV serotype, which can readily pass through the blood–brain barrier in C57BL/6 mice and provide robust brain transgene expression. Mice injected at P30 through the tail vein or retro-orbital sinus showed widespread expression throughout the brain when collected more than 4 weeks later (Fig. 3a,b). To test for off-target effects, we carried out RNA-seq on nuclei from cortical neurons sorted from WT, *Scn2a*$^{+/-}$ and *Scn2a*-rAAV-CRISPRa *Scn2a*$^{+/-}$ PHP.eB rAAV serotype-injected mice using three mice per condition (Methods). We then analysed the mRNA expression of all genes in the same TAD and all *Scn* sodium channel genes. We observed that *Scn2a* showed an upregulated trend that was not significant after correcting for multiple testing in the *Scn2a*-rAAV-CRISPRa *Scn2a*$^{+/-}$-injected mice compared with *Scn2a*$^{+/-}$ -uninjected mice and no other gene in its TAD or *Scn* sodium channel gene showed significant differential expression compared with the WT and *Scn2a*$^{+/-}$ mice (Extended Data Fig. 5a). In contrast to our in vitro RNA-seq, we did not observe any viral response-associated differentially expressed genes (Extended Data Fig. 5b–e). Differentially expressed genes between *Scn2a*-rAAV-CRISPRa *Scn2a*$^{+/-}$-injected and *Scn2a*$^{+/-}$-uninjected mice included *dCas9* and *mCherry* along with a handful of transcripts that represent genes of unknown function. In addition, we analysed sgRNA sequence off-targets with sequences up to three mismatches and two bulges. With these criteria, we found only one putative off-target with three mismatches and two bulges, nearby to a downregulated gene, *Ptchd4*, a negative regulator of the hedgehog pathway[25] (Extended Data Fig. 5f). This gene did not have a significant expression difference

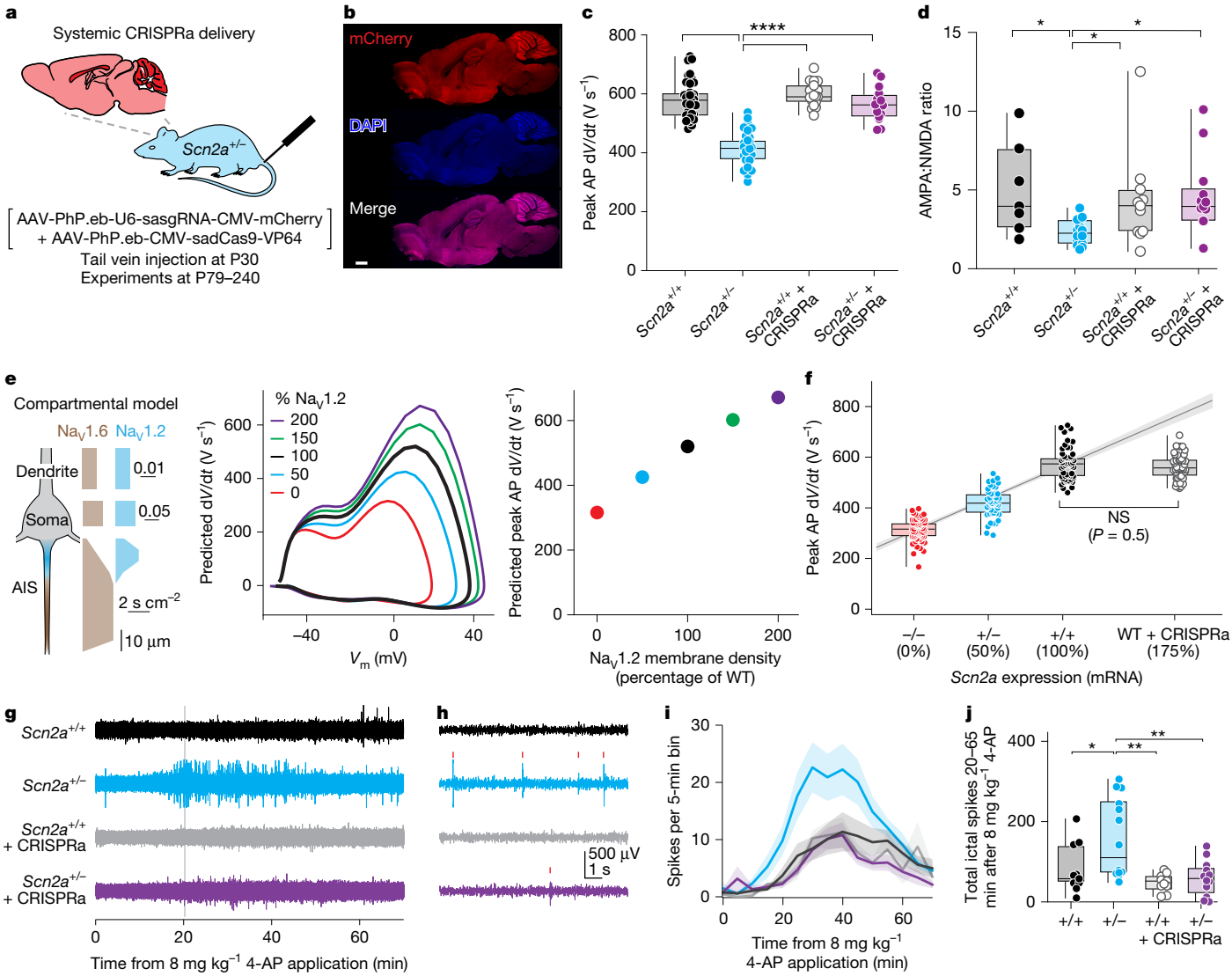

Fig. 3 | Systemic CRT rescues electrophysiological deficits and is protective against chemoconvulsant-induced seizure. a, Schematic of *Scn2a*-rAAV-CRISPRa-PHP.eB intravenous tail vein delivery. Viruses injected described in brackets. **b**, Sagittal brain section from P80 $Scn2a^{+/-}$ + CRISPRa mouse following tail vein injection of *Scn2a*-rAAV-CRISPRa-PHP.eB at P30, stained for mCherry and DAPI. **c**, Peak AP d*V*/d*t* from P82 to P241 $Scn2a^{+/+}$ (black, $n = 44$), $Scn2a^{+/-}$ (cyan, $n = 37$) and tail vein *Scn2a*-rAAV-CRISPRa-PHP.eB-injected $Scn2a^{+/+}$ + CRISPRa (grey, $n = 23$) and $Scn2a^{+/-}$ + CRISPRa (purple, $n = 20$) L5PNs. $^{****}P < 0.0001$, Holm–Šídák multiple comparisons test. **d**, AMPA:NMDA ratio from P79 to P85 $Scn2a^{+/+}$ and $Scn2a^{+/-}$ uninjected controls (left) and P82 to P241 *Scn2a*-CRISPRa-PHP.eB-treated $Scn2a^{+/+}$ and $Scn2a^{+/-}$ mice (right). $n = 7, 14, 11, 13$ cells, respectively. $^{*}P < 0.05$, Holm–Šídák multiple comparisons test versus $Scn2a^{+/-}$. **e**, Left, modelled distribution of $Na_V1.2$ and $Na_V1.6$ across AIS, soma and proximal apical dendrite. Middle, AP phase-plane plots with varying $Na_V1.2$ plasma membrane densities. Right, predicted peak AP d*V*/d*t* as a function of $Na_V1.2$ expression levels. **f**, Empirical measurements of peak AP d*V*/d*t* in $Scn2a^{+/+}$, $Scn2a^{+/-}$ and $Scn2a^{-/-}$ L5PNs compared with $Scn2a^{+/+}$ + CRISPRa. $Scn2a^{+/+}$, $Scn2a^{+/-}$ and $Scn2a^{-/-}$ values are from ref. 24. $Scn2a^{+/+}$ + CRISPRa are merged local and tail vein peak d*V*/d*t* values. Data placed at 175% of WT based on PCR upregulation (Fig. 2c). $Scn2a^{+/+}$ versus $Scn2a^{+/+}$ + CRISPRa; $P = 0.5$, Mann–Whitney test. **g**, EEG from screws placed above PFC in naive or CRISRPa-treated WT and $Scn2a^{+/-}$ mice receiving 8 mg kg^{-1} 4-AP at onset of recording. **h**, Expansion of grey bar area in **g**. Red marks denote automated identification of ictal-like activity. **i**, Ictal spikes, binned per 5 min, across groups. Bars and shading are mean ± s.e.m. **j**, Events per animal at the peak of ictal event period. $^{*}P < 0.03$, $^{**}P < 0.004$, Holm–Šídák multiple comparisons test. Circles are single cells (**c**,**d**,**f**) or animals (**k**); box plots are medians, quartiles and 100% tails. Scale bar, 1 mm.

when comparing *Scn2a*-rAAV-CRISPRa $Scn2a^{+/-}$-injected mice with the WT. Our inability to observe significant upregulation for *Scn2a* in the RNA-seq data from *Scn2a*-rAAV-CRISPRa could be because of its low expression levels and manifestation in specific neuronal cell types[26] as well as the last *Scn2a* exon having high similarity to *Scn1a*, *Scn3a* and *Scn9a* (ranging from 92% to 96% identity). Both attributes probably 'dilute' its expression levels in RNA-seq despite sorting neurons from the cortex. However, we should note that we observed significant upregulation by means of RT–qPCR for *Scn2a* for numerous mice injected with *Scn2a*-rAAV-CRISPRa, through either local or systemic injection (Fig. 2c and Extended Data Fig. 2d), and *Scn2a*-rAAV-CRISPRa dual vector components were detected in the RNA-seq and until 460 days (16 months) by means of RT–qPCR, demonstrating the long-term, persistent AAV transgene expression (Extended Data Fig. 6).

Electrophysiological analysis of *Scn2a*-rAAV-CRISPRa-PHP.eB-injected $Scn2a^{+/-}$ mice showed a rescue of AP peak d*V*/d*t* and AMPA:NMDA ratio, comparable to that of local stereotactic *Scn2a*-rAAV-CRISPRa treatment directly into the mPFC (Fig. 3c,d). Together, these data demonstrate the feasibility of systemic administration of rAAV-CRISPRa to rescue *Scn2a* haploinsufficiency-associated electrophysiological defects.

Scn2a upregulation is well tolerated

Gain-of-function missense variants in *SCN2A* are associated with several forms of epilepsy[2]. Thus, a major concern with a CRISPRa approach to rescue *SCN2A* haploinsufficiency is overexpression beyond normal physiological amounts, as this may result in hyperexcitability, similar to that observed with gain-of-function missense variants. To assess this, we administered CRISPRa intracranially to WT mice and assessed their cellular excitability. Intracranial *Scn2a*-rAAV-CRISPRa injection into mPFC upregulated *Scn2a* mRNA approximately 1.75-fold in WT mice (Fig. 2c). Compartmental models of pyramidal cells predicted that such increases in mRNA, if translated into $Na_V1.2$ channels that incorporate into neuronal membranes, should increase peak dV/dt of APs (Fig. 3e). Indeed, AP velocity in such models was proportional to $Na_V1.2$ membrane density from 0% to 200% of normal levels. In empirical studies, we observed a similar linear relationship between AP peak dV/dt and *Scn2a* copy number between 0% and 100% of normal levels; however, *Scn2a*-rAAV-CRISPRa-treated *Scn2a*$^{+/+}$ cells had peak dV/dt values that were no different than untreated controls (Fig. 3f). This suggests that maximal $Na_V1.2$ function is regulated, perhaps by auxiliary subunits, scaffolding partners and post-translational modifications, and cannot exceed WT levels[12], mirroring similar observations made with other approaches that increase expression of *SCN1A*[27].

CRT suppresses induced seizures

Children with *SCN2A* haploinsufficiency can experience seizures after the first few months of life that are often refractory to treatment[2]. As such, there is a clear unmet need for treatment options that can reduce seizure burden in *SCN2A* haploinsufficiency. At the cellular level, these seizures may be due to loss of $Na_V1.2$ expression in neocortical pyramidal cell dendrites, as marked reductions in *Scn2a* expression can increase intrinsic excitability in these cells through the loss of $Na_V1.2$-supported activation of dendritic potassium channels that contribute to membrane repolarization during APs[24,28]. Furthermore, complete loss of $Na_V1.2$ in layer 5 pyramidal cells is sufficient to generate seizure-like electroencephalography (EEG) activity in mice[29], possibly through their interactions with potassium channels. Given these observations, we tested whether *Scn2a* haploinsufficient mice had increased sensitivity to the chemoconvulsant 4-aminopyridine (4-AP), a non-selective blocker of delayed rectifier potassium channels that drive AP repolarization. *Scn2a*$^{+/-}$ mice exhibited a bias towards seizure-related behavioural activity at earlier times and at lower doses of 4-AP compared with WT (Extended Data Fig. 7). Simultaneous EEG in these mice showed that 4-AP administration, at an intermediate dose (8 mg kg^{-1}), evoked ictal spikes in the frontal cortex that were associated with myoclonic jerking behaviour (Fig. 3g–j and Extended Data Fig. 7). These events peaked in frequency 30–40 min after 4-AP administration, but then subsided within an hour of dosing. At higher doses (15 mg kg^{-1}), ictal spikes often preceded tonic–clonic seizures. To determine whether these seizures could be prevented with our CRT approach, we injected PHP.eB-based *Scn2a*-rAAV-CRISPRa systemically through the retro-orbital sinus at P30 and challenged mice with 8 mg kg^{-1} 4-AP 42–65 days later. Remarkably, ictal spike frequency was reduced to levels observed in naive WT animals in CRT-treated *Scn2a*$^{+/-}$ mice (Fig. 3g–j).

Using whole-cell electrophysiology, we found that CRISPRa-based *Scn2a* mRNA overexpression in WT neurons does not lead to increased $Na_V1.2$ expression in membranes beyond normal WT levels (Fig. 3). Thus, mice should tolerate systemic *Scn2a* overexpression without increased seizure burden. To test this, we injected PHP.eB-based *Scn2a*-rAAV-CRISPRa into WT mice and assessed animal response to 4-AP as in *Scn2a*$^{+/-}$ mice. Ictal spike rates in these mice were comparable to those in untreated WT mice, suggesting that the ceiling placed on $Na_V1.2$ density observed at the cellular level can help to ensure that CRT-based treatments do not inadvertently increase seizure burden.

CRT in human *SCN2A*$^{+/-}$ excitatory neurons

To further investigate the translational potential of this approach, we tested the ability of *SCN2A*-rAAV-CRISPRa to rescue the electrophysiological phenotypes of *SCN2A*$^{+/-}$ neurons differentiated from hESCs. sgRNA constructs that target the human *SCN2A* promoter were designed in a similar strategy to those for mouse and screened for upregulation of *SCN2A* in a human neuroblastoma cell line (SH-SY5Y). One sgRNA out of the ten tested increased *SCN2A* mRNA by 1.5-fold or 1.3-fold following transient co-transfection with dCas9-VP64 or transduction by means of an rAAV-DJ serotype, respectively (Extended Data Fig. 8a,b). *SCN2A*$^{+/+}$ and *SCN2A*$^{+/-}$ hESCs[15] were differentiated into excitatory neurons using the SMADi STEMDiff forebrain differentiation and maturation protocol (Fig. 4a and Methods). Immunostaining of cells at day in vitro (DIV) 65 with MAP2 and GFAP suggested efficient neuronal differentiation alongside supporting glial cells (Fig. 4b).

Early in life, both human and rodent excitatory pyramidal cells rely on $Na_V1.2$ expression in the AIS to support AP electrogenesis[12]. During this period, which persists over the first year in of life in humans, *Scn2a* haploinsufficiency suppresses AP output[13]. As such, CRT can be evaluated in hESCs by examining both AP waveform and AP output. At DIV 65–66, *SCN2A*$^{+/+}$ neurons were mature enough to support repetitive AP activity (Fig. 4c). By contrast, AP electrogenesis was markedly blunted in *SCN2A*$^{+/-}$ neurons, with few evoked APs that had very low peak dV/dt values compared with interleaved controls (Fig. 4d,e). Furthermore, the AISs of these *SCN2A*$^{+/-}$ neurons were approximately 19% longer than those from *SCN2A*$^{+/+}$ counterparts (Extended Data Fig. 9a,b), suggesting that these neurons are responding to reduced excitability by expanding this region associated with AP initiation[12]. *SCN2A*$^{+/-}$ neurons treated with *SCN2A*-rAAV-DJ-CRISPRa at DIV 30 had mRNA levels that were comparable to WT amounts (Extended Data Fig. 8c) and at DIV 65–66 exhibited a full recovery in AP output with a concomitant increase in peak dV/dt (Fig. 4c–e). Moreover, CRISPRa-infected *SCN2A*$^{+/-}$ initial segments were 19% shorter than those of uninfected *SCN2A*$^{+/-}$ neurons visualized in the same preparation, suggesting that AIS structural plasticity was reversed by CRISPRa treatment (Extended Data Fig. 9c,d). In conclusion, these data demonstrate that CRISPRa can provide a potential therapeutic benefit for *SCN2A* haploinsufficiency in human neuronal cell types, rescuing both electrical and structural aspects of neuronal excitability.

Discussion

It is thought that 227 high-confidence NDD-associated genes cause NDDs due to haploinsufficiency, with *SCN2A* haploinsufficiency being one of the most prevalent[4]. Here, we showed how a CRISPRa-based CRT approach could be used to rescue the electrophysiological deficits associated with *SCN2A* haploinsufficiency. First, using a *Cre*-induced rescue of *Scn2a* haploinsufficiency in adolescent mice, we showed the feasibility of this approach to provide a potential therapeutic during adolescence. Next, by direct stereotaxic mPFC and intravenous tail vein injections of *Scn2a*-rAAV-CRISPRa, we upregulated *Scn2a* in adolescent *Scn2a*$^{+/-}$ mice and demonstrated rescue of several features of intrinsic excitability, including AP electrogenesis and associated activation of dendritic calcium channels, as well as synaptic efficacy, as measured by AMPA:NMDA ratio. Of note, these synaptic features were rescued with CRISPRa administration in early adolescence, suggesting both that *Scn2a* haploinsufficiency interrupts normal circuit refinement and that these processes can be reinitiated if normal levels of $Na_V1.2$ are restored. Furthermore, we found that *Scn2a*$^{+/-}$ mice are susceptible to seizure induced by a potassium channel antagonist, and that such seizures can be prevented by CRISPRa treatment. Together,

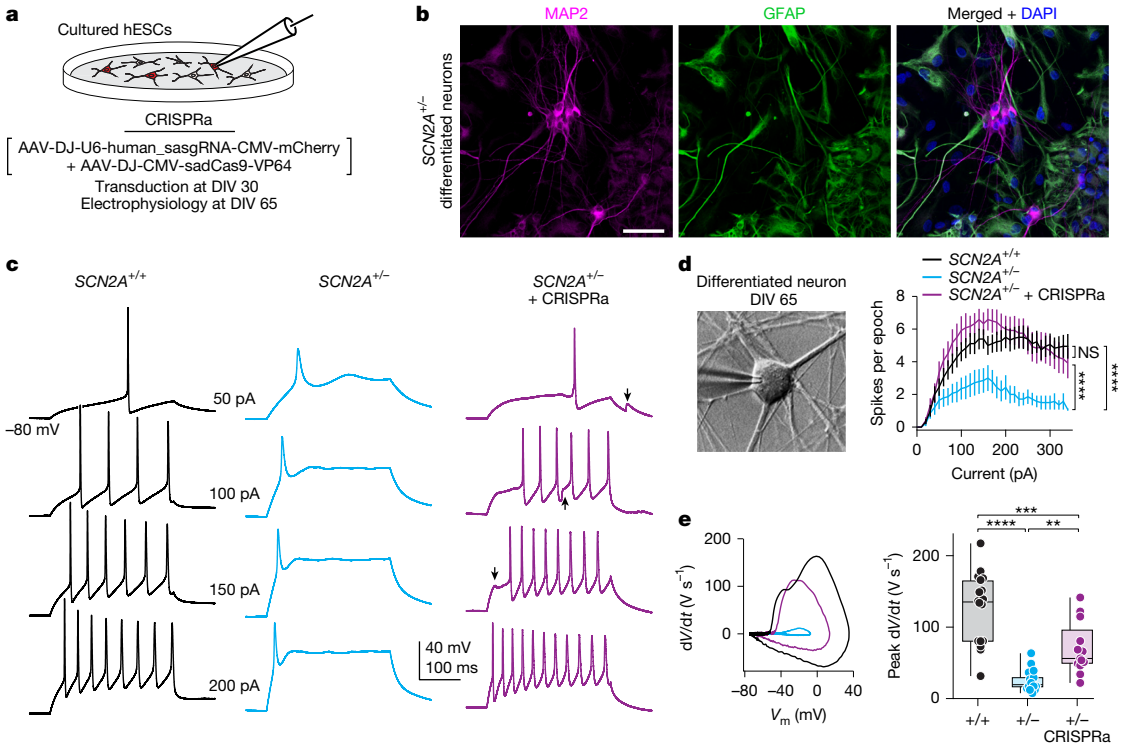

Fig. 4 | *SCN2A*-rAAV-CRISPRa rescues spiking properties of *SCN2A*$^{+/-}$ hESC-derived neurons. a, Schematic of electrophysiological recording of CRISPRa-treated differentiated hESC-derived neurons. Cells were transduced at DIV 30, and experiments were performed at DIV 65–66. **b**, Differentiated *SCN2A*$^{+/-}$ hESC-derived neurons at DIV 65, immunostained with antibodies against the neuronal marker MAP2, the glial marker GFAP and DAPI. **c**, APs generated from a range of current amplitudes (0–340 pA, 10-pA intervals, 300 ms) in DIV 65–66 *SCN2A*$^{+/+}$ (black), *SCN2A*$^{+/-}$ (cyan) and *SCN2A*-rAAV-CRISPRa-treated *SCN2A*$^{+/-}$ (purple) hESC-derived neurons. Arrows highlight spontaneous excitatory postsynaptic potentials that occurred within the recording epoch. **d**, Left, DIC image of *SCN2A*$^{+/-}$ hESC-derived neuron and recording electrode. Right, AP (spikes) per 300-ms stimulation epoch versus current injection amplitude. *SCN2A*$^{+/+}$ versus *SCN2A*$^{+/-}$: ****$P < 0.0001$; *SCN2A*$^{+/-}$ versus *SCN2A*$^{+/-}$ + CRISPRa: ****$P < 0.0001$, Holm–Šídák multiple comparisons test. **e**, Representative phase-plane plots and quantification of peak d*V*/d*t* in *SCN2A*$^{+/+}$, *SCN2A*$^{+/-}$ and *SCN2A*-rAAV-CRISPRa-treated *SCN2A*$^{+/-}$ hESC-derived neurons. $n = 18$ *SCN2A*$^{+/+}$, 18 *SCN2A*$^{+/-}$, 13 *SCN2A*$^{+/-}$ + CRISPRa neurons. **$P = 0.0014$, ***$P = 0.0004$, ****$P < 0.0001$, Holm–Šídák multiple comparisons test. Circles are single cells; box plots are medians, quartiles and 100% tails. Scale bar, 50 µm.

these results indicate that CRT is a viable therapeutic approach for *SCN2A* haploinsufficiency and could be a viable approach to mitigate treatment-refractory seizures observed in this patient population[30].

CRT has been successful in treating rodent models of both CNS and non-CNS haploinsufficiency-related disorders[17,31–38]. In the case of sodium channel haploinsufficiency, CRT also overcomes two of the main limitations of traditional gene replacement therapy, rAAV packaging capacity and ectopic expression. Sodium channels are long genes whose complementary DNA length exceeds the rAAV payload capacity. Classical gene replacement therapy would require splitting the channel into two components using dual AAVs and placing a linker to connect them as was recently used for *Scn1a*[39]. CRT overcomes this limitation by packaging CRISPRa components that target the gene's endogenous regulatory elements to upregulate its expression. In addition, results from a transgenic-based CRISPRa suggest that upregulation occurs only in the tissue/cell type where the targeted regulatory element is active[17], providing further specificity to the rAAV serotype or promoter used to drive expression. In particular, this could be extremely beneficial for sodium channels that have similar protein structures yet have distinct functions in skeletal, cardiac, central nervous and peripheral nervous systems, which make it difficult to target specific isoforms pharmacologically without off-target effects[40,41]. An extra advantage is that CRT uses a nuclease-deficient DNA targeting molecule that does not edit the DNA, and thus off-target effects will not lead to 'DNA scars'. The use of a CRISPR-based CRT approach could lead to immunogenicity due to the dCas9. However, there are many efforts to engineer Cas proteins with reduced immunogenicity by epitope masking[42,43], or by use of alternate Cas proteins, such as those from non-pathogenic bacteria that have not been exposed to humans[10]. Alternatively, other DNA targeting molecules such as zinc fingers or transcription activator-like effector nucleases (TALENS), which should be less immunogenic and smaller in size[44], could be used instead.

A major goal of CRT is to achieve physiological levels of the modulated gene that provide therapeutic benefit. Obtaining levels that are too high could also have deleterious physiological effects, whereas levels too low may not be within the therapeutic window of efficacy. For *SCN2A*, this is of particular importance as gain-of-function variants are associated with epileptic encephalopathies[2]. Here, we intentionally used VP64 as the transcriptional activator to avoid excess $Na_V1.2$ production, as it has modest upregulating potential. Furthermore, we assessed whether *Scn2a* overexpression through CRISPRa above normal physiological conditions affected brain function by upregulating *Scn2a* mRNA in WT mice. Heightened amounts of *Scn2a* mRNA did not correspond to elevated intrinsic or network neuronal hyperexcitability. We speculate that this could be because of a potential ceiling on total $Na_V1.2$ membrane density, perhaps imposed by ancillary subunits, scaffolding partners or post-translational modifications[12], whose regulation remains unchanged. Furthermore, we observed no electrophysiological effects or gene expression changes that would indicate that CRT altered the expression of other CNS sodium channel genes or genes that are in the *Scn2a* TAD region (Extended Data Fig. 3a,b).

Treatments for NDDs would probably be most beneficial when administered early, ideally before symptom onset. Nevertheless, brain development is a dynamic process that spans several decades

of life, and interventions administered even later in life could have some therapeutic benefit[45]. One example is an antisense oligonucleotide therapy for Angelman syndrome that improved communication and motor skills and reduced epileptiform discharges when administered to 4–17-year-old children[46], despite work in rodent models suggesting that therapies should ideally be administered prenatally[47,48]. *Scn2a* haploinsufficiency in mice results in life-long, cell-autonomous impairments in neocortical pyramidal cell dendritic excitability and synapse function[13]. Here, we find that these impairments can be rescued with adolescent reactivation of a LoF allele (Fig. 1) or by CRT-based overexpression through the residual, functional allele (Figs. 2 and 3), suggesting that rescue of normal dendritic excitability can restore many aspects of neuronal function. Future work will help to clarify other *Scn2a*-dependent processes and the critical therapeutic periods needed to address various treatment outcomes across development.

Here, we focused on seizure susceptibility as a primary behavioural outcome measure for CRT. Seizures are a major health concern in the *SCN2A* community, affecting an estimated 20–30% of children with LoF variants, and, by definition, all gain-of-function cases[49]. We found that 4-AP application resulted in a robust, sex-independent increase in ictal spiking in prefrontal cortex (PFC) EEG records that allowed for CRT evaluation in *Scn2a*$^{+/-}$ and safety in WT littermates (Fig. 3g–j). CRT treatment did not lead to any change in seizure burden in 4-AP-treated mice. This is critical, as it suggests that overexpression of *Scn2a* genes can be regulated, avoiding overexpression of $Na_V1.2$ function at neuronal membranes. This places an intrinsic safety factor for *Scn2a* CRT implementation.

In the future, it will be critical to evaluate CRT approaches further with other behaviours that better reflect NDD aspects of *Scn2a* haploinsufficiency. Unfortunately, the field has struggled to identify robust phenotypes in *Scn2a*$^{+/-}$ mice in commonly assessed behaviours[13,50–54]. Leveraging other model systems will probably be critical for assessing proper therapeutic developmental windows and safety profiles. Furthermore, several aspects of this approach will need to be optimized, including safety assessments of rAAV components, off-target CRISPRa effects, the use of non-human primates to assess efficient delivery, upregulation levels, cytotoxicity, immunogenicity and AAV toxicity and serotypes[55,56]. For the latter point, the PHP.eB serotype used here is effective only in specific mouse strains[57], but recently described serotypes that pass the blood–brain barrier in non-human primates[58] or low-intensity focused ultrasound[59] to increase infiltration could potentially be used. In addition, it will be vital to confirm that the *SCN2A* variant to be treated causes a non-functional transcript, as this current approach upregulates both alleles. Last, it is important to note that this therapeutic approach is useful only for variants that lead to a complete LoF allele. Approaches that use allele-specific targeting could potentially be used to overcome this hurdle in cases in which the variant allele does not promote gain-of-function.

In summary, this study shows how CRT using CRISPRa can rescue phenotypes in a genetic mouse model of a prevalent cause of NDDs. CRT is a customizable platform technology that can modify gene expression without directly editing the genome and can be tailored to rescue other disorders caused by haploinsufficiency. The application of CRT to treat *SCN2A* haploinsufficiency leverages a growing understanding of the genetic aetiology of NDDs and demonstrates a potential path forward for treating complex neurodevelopmental conditions through modern genetic medicine approaches.

Online content

Any methods, additional references, Nature Portfolio reporting summaries, source data, extended data, supplementary information, acknowledgements, peer review information; details of author contributions and competing interests; and statements of data and code availability are available at https://doi.org/10.1038/s41586-025-09522-w.

1. Karczewski, K. J. et al. The mutational constraint spectrum quantified from variation in 141,456 humans. *Nature* **581**, 434–443 (2020).
2. Sanders, S. J. et al. Progress in understanding and treating SCN2A-mediated disorders. *Trends Neurosci.* https://doi.org/10.1016/j.tins.2018.03.011 (2018).
3. Maenner, M. J. et al. Prevalence of autism spectrum disorder among children aged 8 years – Autism and Developmental Disabilities Monitoring Network, 11 sites, United States, 2016. *MMWR Surveill. Summ.* https://doi.org/10.15585/MMWR.SS6904A1 (2020).
4. Kaplanis, J. et al. Evidence for 28 genetic disorders discovered by combining healthcare and research data. *Nature* **586**, 757–762 (2020).
5. Fu, J. M. et al. Rare coding variation provides insight into the genetic architecture and phenotypic context of autism. *Nat. Genet.* **54**, 1320–1331 (2022).
6. Epi25 Collaborative Exome sequencing of 20,979 individuals with epilepsy reveals shared and distinct ultra-rare genetic risk across disorder subtypes. *Nat. Neurosci.* **27**, 1864–1879 (2024).
7. Wang, D., Tai, P. W. L. & Gao, G. Adeno-associated virus vector as a platform for gene therapy delivery. *Nat. Rev. Drug Discov.* **18**, 358–378 (2019).
8. Wu, Z., Yang, H. & Colosi, P. Effect of genome size on AAV vector packaging. *Mol. Ther.* **18**, 80–86 (2010).
9. Howe, K. L. et al. Ensembl 2021. *Nucleic Acids Res.* **49**, D884–D891 (2021).
10. Matharu, N. & Ahituv, N. Modulating gene regulation to treat genetic disorders. *Nat. Rev. Drug Discov.* **19**, 757–775 (2020).
11. Werling, D. M. et al. Whole-genome and RNA sequencing reveal variation and transcriptomic coordination in the developing human prefrontal cortex. *Cell Rep.* **31**, 107489 (2020).
12. Jenkins, P. M. & Bender, K. J. Axon initial segment structure and function in health and disease. *Physiol. Rev.* **105**, 765–801 (2025).
13. Spratt, P. W. E. et al. The autism-associated gene Scn2a contributes to dendritic excitability and synaptic function in the prefrontal cortex. *Neuron* **103**, 673–685 (2019).
14. Nelson, A. D. et al. Physical and functional convergence of the autism risk genes Scn2a and Ank2 in neocortical pyramidal cell dendrites. *Neuron* **112**, 1133–1149 (2024).
15. Lu, C. et al. Overexpression of NEUROG2 and NEUROG1 in human embryonic stem cells produces a network of excitatory and inhibitory neurons. *FASEB J.* **33**, 5287–5299 (2019).
16. Li, T. et al. Action potential initiation in neocortical inhibitory interneurons. *PLoS Biol.* https://doi.org/10.1371/journal.pbio.1001944 (2014).
17. Matharu, N. et al. CRISPR-mediated activation of a promoter or enhancer rescues obesity caused by haploinsufficiency. *Science* **363**, eaau0629 (2019).
18. Grimm, D. et al. In vitro and in vivo gene therapy vector evolution via multispecies interbreeding and retargeting of adeno-associated viruses. *J. Virol.* **82**, 5887–5911 (2008).
19. Bae, S., Park, J. & Kim, J.-S. Cas-OFFinder: a fast and versatile algorithm that searches for potential off-target sites of Cas9 RNA-guided endonucleases. *Bioinformatics* **30**, 1473–1475 (2014).
20. Wang, W. et al. PTPN14 is required for the density-dependent control of YAP1. *Genes Dev.* **26**, 1959–1971 (2012).
21. Correia, J. C. et al. Zfp697 is an RNA-binding protein that regulates skeletal muscle inflammation and remodeling. *Proc. Natl Acad. Sci. USA* **121**, e2319724121 (2024).
22. Busse, D. C. et al. Interferon-induced protein 44 and interferon-induced protein 44-like restrict replication of respiratory syncytial virus. *J. Virol.* **94**, e00297–20 (2020).
23. Baum, M. L. et al. CSMD1 regulates brain complement activity and circuit development. *Brain Behav. Immun.* **119**, 317–332 (2024).
24. Spratt, P. W. E. et al. Paradoxical hyperexcitability from NaV1.2 sodium channel loss in neocortical pyramidal cells. *Cell Rep.* **36**, 109483 (2021).
25. Chung, J. H., Larsen, A. R., Chen, E. & Bunz, F. A PTCH1 homolog transcriptionally activated by p53 suppresses hedgehog signaling. *J. Biol. Chem.* **289**, 33020–33031 (2014).
26. Liang, L. et al. Developmental dynamics of voltage-gated sodium channel isoform expression in the human and mouse brain. *Genome Med.* **13**, 135 (2021).
27. Yuan, Y. et al. Antisense oligonucleotides restore excitability, GABA signalling and sodium current density in a Dravet syndrome model. *Brain* **147**, 1231–1246 (2024).
28. Zhang, J. et al. Severe deficiency of the voltage-gated sodium channel NaV1.2 elevates neuronal excitability in adult mice. *Cell Rep.* **36**, 109495 (2021).
29. Miyamoto, H. et al. Impaired cortico-striatal excitatory transmission triggers epilepsy. *Nat. Commun.* **10**, 1917 (2019).
30. Reynolds, C., King, M. D. & Gorman, K. M. The phenotypic spectrum of SCN2A-related epilepsy. *Eur. J. Paediatr. Neurol.* **24**, 117–122 (2020).
31. Colasante, G. et al. dCas9-based Scn1a gene activation restores inhibitory interneuron excitability and attenuates seizures in Dravet syndrome mice. *Mol. Ther.* **28**, 235–253 (2020).
32. Colasante, G. et al. In vivo CRISPRa decreases seizures and rescues cognitive deficits in a rodent model of epilepsy. *Brain* **143**, 891–905 (2020).
33. Yamagata, T. et al. CRISPR/dCas9-based Scn1a gene activation in inhibitory neurons ameliorates epileptic and behavioral phenotypes of Dravet syndrome model mice. *Neurobiol. Dis.* **141**, 104954 (2020).
34. Chang, H.-C. et al. rAAV-CRISPRa therapy corrects Rai1 haploinsufficiency and rescues selective disease features in Smith–Magenis syndrome mice. *J. Biol. Chem.* **299**, 102728 (2023).
35. Wang, G. et al. Multiplexed activation of endogenous genes by CRISPRa elicits potent antitumor immunity. *Nat. Immunol.* **20**, 1494–1505 (2019).
36. Liao, H.-K. et al. In vivo target gene activation via CRISPR/Cas9-mediated trans-epigenetic modulation. *Cell* **171**, 1495–1507 (2017).
37. Böhm, S. et al. A gene therapy for inherited blindness using dCas9-VPR-mediated transcriptional activation. *Sci. Adv.* **6**, eaba5614 (2020).
38. Kemaladewi, D. U. et al. A mutation-independent approach for muscular dystrophy via upregulation of a modifier gene. *Nature* **572**, 125–130 (2019).
39. Mich, J. K. et al. Interneuron-specific dual-AAV SCN1A gene replacement corrects epileptic phenotypes in mouse models of Dravet syndrome. *Sci. Transl. Med.* **17**, eadn5603 (2025).
40. Waszkielewicz, A. M. et al. Ion channels as drug targets in central nervous system disorders. *Curr. Med. Chem.* **20**, 1241–1285 (2013).

41. Johnson, J. P. et al. NBI-921352, a first-in-class, NaV1.6 selective, sodium channel inhibitor that prevents seizures in Scn8a gain-of-function mice, and wild-type mice and rats. *eLife* **11**, e72468 (2022).
42. Ferdosi, S. R. et al. Multifunctional CRISPR-Cas9 with engineered immunosilenced human T cell epitopes. *Nat. Commun.* **10**, 1842 (2019).
43. Mehta, A. & Merkel, O. M. Immunogenicity of Cas9 protein. *J. Pharm. Sci.* **109**, 62–67 (2020).
44. Gaj, T., Sirk, S. J., Shui, S.-L. & Liu, J. Genome-editing technologies: principles and applications. *Cold Spring Harb. Perspect. Biol.* **8**, a023754 (2016).
45. Levy, G. & Barak, B. Postnatal therapeutic approaches in genetic neurodevelopmental disorders. *Neural Regen. Res.* **16**, 414–422 (2021).
46. Markati, T., Duis, J. & Servais, L. Therapies in preclinical and clinical development for Angelman syndrome. *Expert Opin. Investig. Drugs* **30**, 709–720 (2021).
47. Silva-Santos, S. et al. Ube3a reinstatement identifies distinct developmental windows in a murine Angelman syndrome model. *J. Clin. Invest.* **125**, 2069–2076 (2015).
48. Wolter, J. M. et al. Cas9 gene therapy for Angelman syndrome traps Ube3a-ATS long non-coding RNA. *Nature* **587**, 281–284 (2020).
49. Berg, A. T. et al. Expanded clinical phenotype spectrum correlates with variant function in SCN2A-related disorders. *Brain* **147**, 2761–2774 (2024).
50. Eaton, M. et al. Generation and basic characterization of a gene-trap knockout mouse model of Scn2a with a substantial reduction of voltage-gated sodium channel Nav 1.2 expression. *Genes Brain Behav.* **20**, e12725 (2021).
51. Tatsukawa, T. et al. Scn2a haploinsufficient mice display a spectrum of phenotypes affecting anxiety, sociability, memory flexibility and ampakine CX516 rescues their hyperactivity. *Mol. Autism* **10**, 15 (2019).
52. Shin, W. et al. Scn2a haploinsufficiency in mice suppresses hippocampal neuronal excitability, excitatory synaptic drive, and long-term potentiation, and spatial learning and memory. *Front. Mol. Neurosci.* **12**, 145 (2019).
53. Léna, I. & Mantegazza, M. NaV1.2 haploinsufficiency in Scn2a knock-out mice causes an autistic-like phenotype attenuated with age. *Sci. Rep.* **9**, 12886 (2019).
54. Schamiloglu, S., Wu, H., Zhou, M., Kwan, A. C. & Bender, K. J. Dynamic foraging behavior performance is not affected by Scn2a haploinsufficiency. *eNeuro* **10**, ENEURO.0367-23.2023 (2023).
55. Goertsen, D. et al. AAV capsid variants with brain-wide transgene expression and decreased liver targeting after intravenous delivery in mouse and marmoset. *Nat. Neurosci.* **25**, 106–115 (2022).
56. Keiser, M. S. et al. Toxicity after AAV delivery of RNAi expression constructs into nonhuman primate brain. *Nat. Med.* **27**, 1982–1989 (2021).
57. Hordeaux, J. et al. The GPI-linked protein LY6A drives AAV-PHP.B transport across the blood-brain barrier. *Mol. Ther.* **27**, 912–921 (2019).
58. Yao, Y. et al. Variants of the adeno-associated virus serotype 9 with enhanced penetration of the blood-brain barrier in rodents and primates. *Nat. Biomed. Eng.* **6**, 1257–1271 (2022).
59. Blesa, J. et al. BBB opening with focused ultrasound in nonhuman primates and Parkinson's disease patients: targeted AAV vector delivery and PET imaging. *Sci. Adv.* **9**, eadf4888 (2023).

Methods

CRISPRa in vitro optimization

Ten sgRNAs targeting the mouse *Scn2a* or human *SCN2A* promoters were designed using the Broad Institute's GPP sgRNA Design Tool (Genetic Perturbation Platform, Broad Institute). These guides were individually cloned into pAAV-U6-sasgRNA-CMV-mCherry-WPREpA (Addgene, 217015) at the *BstX*I and *Xho*I restriction enzyme sites using the In-Fusion HD cloning kit (Clontech). rAAV vectors were generated using similar plasmids and cloning methods as described previously[1]. Mouse sgRNAs were tested in the neuroblastoma cell line Neuro-2a (ATCC CCL-131). Cells were grown in Dulbecco's modified Eagle's medium with 10% FBS and 1% penicillin-streptomycin, and SH-SY5Y cells were grown in Eagle's minimum essential medium with 10% FBS and 1% penicillin-streptomycin, following ATCC guidelines. Cells were transiently co-transfected with individual sgRNAs cloned into pAAV-U6-sasgRNA-CMV-mCherry-WPREpA along with pCMV-sadCas9-VP64 (Addgene, 115790) for 48 h using Opti-MEM Reduced Serum Medium (Thermo Fisher) and X-tremeGENE HP (Sigma-Aldrich). RNA was isolated using the RNeasy Mini Kit (Qiagen) following the manufacturer's protocol. cDNA was synthesized using SuperScript III First-Strand Synthesis System (Invitrogen) and qPCR was conducted using SsoFast EvaGreen Supermix (Bio-Rad) and analysed using the $\Delta\Delta C_T$ methods, comparing with a no-sgRNA transfection and normalized to *Actb* as a housekeeping gene. rAAVs were produced at the Stanford Gene Vector and Viral Core (see Supplementary Table 3 for genomic titre).

RNA-seq

For cell culture RNA-seq, we used two biological replicates and three technical replicates for each condition (six samples per condition) from Neuro-2a treated with either rAAV-sadCas9-VP64 (negative control) or rAAV-sadCas9-VP64 + rAAV-*Scn2a*-sgRNA. For mouse RNA-seq, cortices were dissected from WT and heterozygous mice, with or without rAAV-sadCas9-VP64 + rAAV-*Scn2a*-sgRNA injection, three mice per condition. For each sample, nuclei were isolated from approximately 200 mg of cortex using the Singulator 100 System (S2 Genomics) with the Single Shot Standard Nuclei Isolation v.2 program. The isolation was performed in 3 ml of lysis buffer (10 mM Tris-HCl, pH 7.4; 10 mM NaCl; 3 mM $MgCl_2.6H_2O$; 0.05% IGEPAL CA-630; 0.5 mM DTT; nuclease-free water) and 3 ml of wash buffer (5% BSA, 0.25% glycerol in 1× PBS). To preserve RNA integrity, 50 µl of Protector RNase Inhibitor (Sigma-Aldrich, 3335402001) was added directly to the Singulator cartridge. Following isolation, nuclei were centrifuged, and debris were removed by centrifugation in wash buffer supplemented with 1× Nuclei Debris Removal Stock Reagent (S2 Genomics, 100253628) and 37.5 µl of RNase inhibitor at 600*g* for 15 min at 4 °C, with deceleration set to 1. Purified nuclei were then washed once in wash buffer and resuspended in 500 µl of wash buffer supplemented with 6.5 µl of Protector RNase Inhibitor, DAPI (Biotium, 40043; 1:1,000) and anti-NeuN-488 antibody (Sigma-Aldrich, MAB377X; 1:500). The suspension was incubated for 1 h at 4 °C in the dark to allow staining. Finally, nuclei were washed once with wash buffer, resuspended in 1 ml of wash buffer supplemented with 12.5 µl of Protector RNase Inhibitor and transferred to a FACS tube. Neuronal nuclei were sorted on the basis of DAPI and NeuN positivity using a BD FACSAria™ II (BD Biosciences) (Extended Data Fig. 5g–i). Sorted nuclei were then resuspended in 700 µl of QIAzol lysis reagent (Qiagen, 79306), and total RNA was extracted using the miRNeasy kit (Qiagen, 217084) following the manufacturer's instructions. Extracted RNA was sent to Novogene for mRNA library preparation (polyA enrichment) and sequenced using a NovaSeq 6000, generating 150-bp end reads.

RNA-seq reads were trimmed on the 3′ ends of reads for which the quality score was less than 20 using trim galore 0.6.10 through nf-core RNA-seq pipeline v.3.18 (ref. 60). In brief, sequences were mapped to mm39 with STAR 2.7.8a (ref. 61) and counts were computed using featureCounts with gtf provided from Ensembl (Mus_musculus.GRCm39.113). Post alignment, gene annotation was carried out using Ensembl Transcripts release 113. Genes exhibiting a maximum count of one or less were removed. The remaining gene counts were normalized to counts per million. Differential expression was characterized using DESeq2 v.1.44 (2024-05-01)[61] and R v.4.4. Genes with an average normalized count of less than one across all samples were considered not significantly different. Gene ontology over-representation analysis using GSEApy v.1.1.3 (ref. 62) was performed on significantly upregulated genes. Upregulated genes were tested for gene ontology term enrichment against a background of genes expressed in the RNA-seq samples using Fisher's exact test for statistical significance. Benjamini–Hochberg multiple testing correction was performed and gene ontology terms with an adjusted *P* value less than 0.05 were considered significantly enriched. All RNA-seq data are available on the NCBI Gene Expression Omnibus as Bioproject PRJNA1292778.

Mouse generation, husbandry and genotyping

All mouse work was approved by the University of California, San Francisco Institutional Animal Care and Use Committee. All mice were maintained on a C57BL/6J background on a 12:12 light–dark cycle (light on at 6.00 a.m.) with ad libitum food and water, with daily health monitoring. Genotyping was performed by means of tail clips using the KAPA Mouse Genotyping Kit (Roche, 07961766001). See Supplementary Table 2 for primer sequences. $Scn2a^{+/-}$ were as described in ref. 63; conditional knockout ($Scn2a^{+/fl}$) were as described in ref. 13. $Scn2a^{+/KI}$ mice were created at Cyagen Biosciences by inverting exons 3–5 of the *Scn2a* gene and inserting an SA-2A-eGFP-polyA cassette upstream of the inverted exons. The inverted exons and the SA-2A-eGFP-polyA cassette were flanked with loxP and Lox2272 sites to ensure the excision of the SA-2A-eGFP-polyA cassette and the reversion of exons 3–5 to the correct orientation following Cre recombinase-induced recombination. A targeting vector containing the inverted exons, SA-2A-eGFP-polyA cassette, recombination sites, selection markers and homology arms was assembled from mouse genomic fragments amplified from BAC clones RP23-332C13 and RP23-55C23. The targeting vector was linearized by restriction enzyme digestion and transfected into C57BL/6 embryonic stem cells through electroporation, and successfully transfected cells were identified by drug selection, PCR verification and Southern blot confirmation. Confirmed clones were introduced into host embryos and transferred to surrogate mothers. Chimerism in the resulting pups was identified by means of coat colour. F0 male chimeras were bred with C57BL/6J females to generate F1 heterozygous mutants that were identified by PCR.

In vivo AAV administration

For local AAV administration, mice aged P30–P40 were kept under live anaesthetic isoflurane at 0.5–2.0% and mounted onto the stereotaxic machine (Kopf 1900). Then, 500 nl of rAAV at a 1:1 ratio of sgRNA and sadCas9-VP64 or 1 µl of EF1α-Cre-mCerry was injected into the mPFC at stereotaxic coordinates (mm): anterior-posterior, +1.7; mediolateral, −0.35; dorsoventral, −2.6, at a viral infusion rate of 0.1 µl min^{-1}. For systemic AAV administration, mice aged P30–P40 were kept on a 37 °C warm pad and harnessed using a brass mouse restrainer (SAI Infusion Tech). Lateral tail vein injections were carried out with rAAV at a 1:1 ratio of sgRNA and sadCas9-VP64 (1×10^{11} viral genomes per mouse) suspended in 200 µl of saline using a 30 G needle. For either injection, mice were used for subsequent experiments 4 weeks after injection. Tail-vein-injected animals used for EEG recording experiments were subsequently divided across experiments for electrophysiological recordings, RT–qPCR and immunofluorescence.

In vivo dissections

At 4 weeks after injection, mouse brains were removed and 250-µm-thick coronal slices containing the mPFC were dissected in artificial cerebrospinal solution containing (in mM): 87 NaCl, 25 $NaHCO_3$,

25 glucose, 75 sucrose, 2.5 KCl, 1.25 NaH_2PO_4, 0.5 $CaCl_2$ and 7 $MgCl_2$; bubbled with 5%CO_2/95%O_2; 4 °C. Fluorescence mCherry expression in the mPFC of the injected hemisphere was validated using a fluorescence stereomicroscope (Nikon SMZ1500). For mRNA expression analyses, both the injected (mCherry-positive) and uninjected hemispheres (mCherry-negative) were dissected using a sterile Miltex disposable punch biopsy (Medline MIL3332P25) and flash-frozen in RLT lysis buffer (Qiagen). RNA was extracted using the RNAEasy Micro Kit (Qiagen) following the manufacturer's protocol. cDNA and downstream qPCR were conducted using SuperScript III (Invitrogen) and SsoFast EvaGreen Supermix (Bio-Rad) on a QuantStudio 6 Flex Real Time PCR system (Applied Biosystems). qPCR results comparing the injected and uninjected hemispheres were analysed using the $\Delta\Delta C_T$ methods and normalized to *Actb*, a housekeeping gene.

Ex vivo electrophysiology and two-photon imaging

All ex vivo electrophysiology and two-photon imaging were acquired and performed using the same methods as described previously[13,24]. Mice were anaesthetized using isoflurane and 250-µm coronal slices were prepared. Cutting solution contained (in mM): 87 NaCl, 25 $NaHCO_3$, 25 glucose, 75 sucrose, 2.5 KCl, 1.25 NaH_2PO_4, 0.5 $CaCl_2$ and 7 $MgCl_2$; bubbled with 5%CO_2/95%O_2; 4 °C. Following cutting, slices were incubated either in the same solution or in the recording solution for 30 min at 33 °C, then at room temperature until recording. Recording solution contained (in mM): 125 NaCl, 2.5 KCl, 2 $CaCl_2$, 1 $MgCl_2$, 25 $NaHCO_3$, 1.25 NaH_2PO_4, 25 glucose; bubbled with 5%CO_2/95%O_2; 32–34 °C, approximately 310 mOsm. Neurons were visualized with DIC optics for conventional visually guided whole-cell recording, or Dodt contrast imaging, or with two-photon-guided imaging of reporter-driven mCherry or GFP fluorescence overlaid on an image of the slice (scanning DIC). Cells of interest were chosen on the basis of fluorescence expression in all experiments in *Scn2a*$^{+/KI}$ mice and in all experiments using CRISPRa constructs. For current-clamp recordings, patch electrodes (Schott 8250 glass, 3–4-MΩ tip resistance) were filled with a solution containing (in mM): 113 K-gluconate, 9 HEPES, 4.5 $MgCl_2$, 0.1 EGTA, 14 $Tris_2$-phosphocreatine, 4 Na_2-ATP, 0.3 Tris-GTP; approximately 290 mOsm, pH 7.2–7.25. For Ca^{2+} imaging, EGTA was replaced with 250 µM Fluo-5F and 20 µM Alexa 594. For voltage-clamp recordings of synaptic activity, internal solution contained (in mM): 110 $CsMeSO_3$, 40 HEPES, 1 KCl, 4 NaCl, 4 Mg-ATP, 10 Na-phosphocreatine, 0.4 Na_2-GTP, 0.1 EGTA; approximately 290 mOsm, pH 7.22. All data were corrected for measured junction potentials of 12 and 11 mV in K- and Cs-based internals, respectively.

Electrophysiological data were acquired using Multiclamp 700A or 700B amplifiers (Molecular Devices) by means of custom routines in IgorPro (Wavemetrics). For measurements of AP waveform, data were acquired at 50 kHz and filtered at 20 kHz. For all other measurements, data were acquired at 10–20 kHz and filtered at 3–10 kHz. For current-clamp recordings, pipette capacitance was compensated by 50% of the fast capacitance measured under gigaohm seal conditions in voltage-clamp before establishing a whole-cell configuration, and the bridge was balanced. For voltage-clamp recordings, pipette capacitance was compensated completely, and series resistance was compensated 50%. Series resistance was less than 15 MΩ in all recordings. Experiments were omitted if input resistance changed by more than ±15%.

2PLSM was performed as previously described[13]. A two-photon source (Coherent Ultra II) was tuned to 810 nm for morphology and calcium imaging. Epi- and trans-fluorescence signals were captured either through a ×40, 0.8 numerical aperture (NA) objective for calcium imaging or with a ×60, 1.0 NA objective for spine morphology imaging, paired with a 1.4 NA oil immersion condenser (Olympus). Fluorescence was split into red and green channels using dichroic mirrors and band-pass filters (575 DCXR, ET525/70m-2p, ET620/60m-2p, Chroma). Green fluorescence (Fluo-5F) was captured with 10770–40 photomultiplier tubes selected for high quantum efficiency and low dark counts (Hamamatsu). Red fluorescence (Alexa 594) was captured with R9110 photomultiplier tubes. Data were collected in linescan mode (2–2.4 ms per line, including mirror flyback). For calcium imaging, data were presented as averages of 10–20 events per site and expressed as $\Delta G/G_{sat} \times 100$, where G_{sat} was the maximal fluorescence in saturating Ca^{2+} (2 mM). AP backpropagation experiments were performed in 25 µM picrotoxin, 10 µM NBQX and 10 µM R-CPP.

EEG implant surgeries

Mice were anaesthetized with isoflurane and placed on a stereotaxic apparatus. Screws with wire leads were implanted in 2–3 turns into five burr holes at (stereotaxic coordinates relative to bregma (mm)): PFC: 1.7 anterior-posterior, −0.3 mediolateral; S1: −1.8 anterior-posterior, 2.5 mediolateral; reference and ground: −5 anterior-posterior, 0.9 mediolateral (Pinnacle Technology). A head mount was then attached to the wire leads and secured in adhesive dental cement. Mice were given at least 1 week for post-surgery recovery before EEG recordings.

EEG recordings and analysis

EEG recordings were performed using the Sirenia Acquisition Software (Pinnacle Technology) at 2-kHz sampling frequency with simultaneous video capture. 4-AP doses at 6 and 8 mg kg^{-1} were delivered in sessions spaced at least 2 d apart. We administered 15 mg kg^{-1} at least 1 week thereafter. 4-AP was prepared fresh at the start of every recording day. Recordings were performed between 10.00 a.m. and 6.00 p.m. to control for the circadian light–dark cycle. EEG analyses were performed with custom routines in IgorPro based on deconvolution-based event detection for spontaneous synaptic activity as described previously[6]. A series of ictal spike events from EEG screws placed above the frontal cortex were averaged to create a 100-ms template event for all subsequent analyses. Ictal spikes were identified as all events with a deconvolved signal 3.5× above background noise.

Behavioural seizure scoring was made from simultaneous video and EEG monitoring. Behavioural classification of increasing seizure severity was based on the Racine scale and a previous report of seizures in *Scn2a*$^{+/-}$ mice[29,64]. Latency to seizure activity was considered the time from 4-AP administration to the onset of the first seizure. Behavioural arrest was defined as a sudden immobilization of the animal. A myoclonic jerk was defined as a neck or body twitch accompanied by a single sharp spike in the EEG signal. A tonic–clonic seizure was defined as clonic convulsions leading to wild jumping also with high-amplitude spiking in the EEG signal. The animal was considered deceased when the tonic–clonic seizure led to tonic extension of hind limbs followed by loss of body tone and close to flat EEG signal.

Computational compartmental modelling

A pyramidal cell compartmental model was implemented in the NEURON environment (v.7.7) based on the Blue Brain Project thick-tufted layer 5b pyramidal cell (TTPC1) model used in our previous study[24,65,66]. The TTPC1 model was adjusted to include an AIS, and the original Na channels in the TTPC1 model were replaced with $Na_V1.2$ and $Na_V1.6$ channels in compartments with densities as described previously[24].

hESC differentiation, maturation and electrophysiology

WT and *SCN2A*$^{+/-}$ HUES66 (NIH Registration 0057) hESC cell lines were obtained from the Harvard Stem Cell Institute and plated on Matrigel (Corning)-coated standard tissue culture plates maintained in mTESR (STEMCELL). Neural progenitor cell hESCs were differentiated following the manufacturer's instructions using the STEMDiff SMADi Embryoid Body Neural Induction protocol (STEMCELL), following a similar strategy to one documented previously[67]. Neural progenitor cells were further differentiated into neuronal forebrain precursors using the STEMdiff ForeBrain Neuron Differentiation protocol (Document

10000005464, STEMCELL, CanadaSTEMcell Tech), and neuronal precursors were matured into forebrain neurons using the STEMdiff Forebrain Maturation Kit with BrainPhys (STEMCELL). Neuronal precursors were maturated on poly-L-ornithine laminin-coated German glass coverslips (Neuvitro GG-25-1.5-Laminin) for 65 d. Whole-cell current-clamp recordings were done as in mouse acute slices, using identical solutions.

Immunofluorescence of fixed cells or tissue

For hESCs, differentiated neurons were fixed at DIV 65 with 4% paraformaldehyde and 4% sucrose and blocked with 10% normal goat serum in PBS in 0.2% Triton-X. All coverslips within a set of experiments, including those used previously that day for electrophysiology, were fixed within 1 h of each other to minimize developmental differences across coverslips. Following fixation, cells were incubated with primary antibodies against MAP2 (Invitrogen, PA1-10005) at 1:5,000 and Ankyrin-G (Neuromab, 75-146) at 1:1,000 overnight at 4 °C. Cells were then incubated with the secondary antibodies Goat anti-Chicken IgY (H+L) Cross-Absorbed Secondary Antibody, Alexa Fluor Plus 647 (Invitrogen, A32933) at 1:500 and Goat anti-Mouse IgG (H+L) Highly Cross Adsorbed Secondary Antibody, Alexa Fluor 488 (Thermo Fisher, A-11029) at 1:500. They were then mounted on coverslips with ProLong Diamond Antifade Mountant with DAPI (Thermo Fisher). Images were captured with a ×40, 1.4 NA objective using an Olympus Fluoview FV3000 confocal microscope. AIS length was measured from maximum intensity projections generated from z-stacks that contained the entire bounds of the neuron based on ankyrin-G and MAP2 immunofluorescence. Only initial segments with clearly detectable start and end points were quantified using the segmented line tool in FIJI (ImageJ). Start and end points were determined with a threshold of 50% peak ankyrin-G fluorescence intensity using plot profiles (pixel intensity/distance) in FIJI.

For whole-brain mouse immunohistochemistry, mice were perfused with 4% paraformaldehyde in PBS and brains were removed and sectioned coronally or sagittally on a vibratome (Leica, VT1000) at 50–75 µm, and then mounted on slides with ProLong Gold Antifade Mountant with DAPI. For imaging of *Scn2a*$^{+/KI}$ sections, tissue was permeabilized, blocked and immunostained for GFP (anti-GFP AlexaFluor 488, 1:500, ThermoFisher A-21311) and parvalbumin (PV27, 1:500, Swant; AlexaFluor 564 secondary, 1:500, ThermoFisher). Sections were imaged with either an Olympus Fluoview FV3000 (coronal sections) or a Keyence BZ-X widefield microscope (sagittal sections).

Quantification and statistical analysis

Unless otherwise noted, all data are shown in figures as box plots, with median and quartiles and minimum and maximum tails, with individual data points overlaid, or as mean ± standard error with individual data points overlaid. A Kruskal–Wallis non-parametric test with Holm–Šídák multiple comparisons testing was performed unless otherwise noted. Statistical tests are noted in figure legends. All tests used were two-sided. Results were considered significant at an alpha value of $P < 0.05$. For multiple comparisons tests used to compare several conditions, no indication of significance in the figure means not significant. Statistical analysis was performed using Prism 9 (GraphPad). For electrophysiology and imaging experiments, acute slices were typically generated blind to genotype and experiments were interleaved between two or three genotypes/injection conditions to control for recording conditions. Group sample sizes were chosen on the basis of standards in the field and previous similar experiments conducted by our group[13,24]. No statistical methods were used to predetermine sample size. A minimum of two biological replicates were tested in all experiments.

Reporting summary

Further information on research design is available in the Nature Portfolio Reporting Summary linked to this article.

Data availability

All RNA-seq data are available at the NCBI Gene Expression Omnibus as Bioproject GSE302897. Requests for materials can be directed to N.A. (CRT-based approaches) or K.J.B. (mouse models). Source data are provided with this paper.

Code availability

No custom code was generated for this work.

60. Ewels, P. A. et al. The nf-core framework for community-curated bioinformatics pipelines. *Nat. Biotechnol.* **38**, 276–278 (2020).
61. Love, M. I., Huber, W. & Anders, S. Moderated estimation of fold change and dispersion for RNA-seq data with DESeq2. *Genome Biol.* **15**, 550 (2014).
62. Fang, Z., Liu, X. & Peltz, G. GSEApy: a comprehensive package for performing gene set enrichment analysis in Python. *Bioinformatics* **39**, btac757 (2023).
63. Planells-Cases, R. et al. Neuronal death and perinatal lethality in voltage-gated sodium channel α_{II}-deficient mice. *Biophys. J.* **78**, 2878–2891 (2000).
64. Van Erum, J., Van Dam, D. & De Deyn, P. P. PTZ-induced seizures in mice require a revised Racine scale. *Epilepsy Behav.* **95**, 51–55 (2019).
65. Markram, H. et al. Reconstruction and simulation of neocortical microcircuitry. *Cell* **163**, 456–492 (2015).
66. Ben-Shalom, R. et al. Opposing effects on NaV1.2 function underlie differences between SCN2A variants observed in individuals with autism spectrum disorder or infantile seizures. *Biol. Psychiatry* **82**, 224–232 (2017).
67. Ruden, J. B., Dixit, M., Zepeda, J. C., Grueter, B. A. & Dugan, L. L. Robust expression of functional NMDA receptors in human induced pluripotent stem cell-derived neuronal cultures using an accelerated protocol. *Front. Mol. Neurosci.* **14**, 777049 (2021).

Acknowledgements We thank the Bender and Ahituv laboratory members for comments and discussions on this manuscript, and members of the FamilieSCN2A Foundation who provided the core motivation and inspiration for this work. We acknowledge the UCSF Parnassus Flow CoLab (RRID:SCR_018206) supported in part by NIH grant no. P30 DK063720 and by the NIH S10 Instrumentation Grant no. S10 1S10OD021822-01. This work was supported by grants from SFARI (grant no. 629287: K.J.B., N.A.; grant no. 513133: K.J.B.), the Broad Institute Target Practice Initiative (K.J.B.), the Autism Science Foundation (S.T.), the Weill Neurohub Investigator Program (K.J.B., N.A.), an NSERC Predoctoral Fellowship (P.W.E.S.), the Ford Foundation Dissertation Fellowship (S.S.H.), the Weill Foundation Graduate Student Fellowship (S.S.H.), an NSF Graduate Fellowship (S.T.) and the NIH (grant no. R01 MH125978: K.J.B.; grant no. R01 MH136475: K.J.B., N.A.; grant nos. F32 MH125536 and K99 MH135209: A.D.N.; grant nos. R01 NS078118 and R01 NS121287: J.T.P.; grant no. R01 MH115045, R01 NS108874 and R01 MH118298: J.Q.P.; grant no. T32 GM007449: S.S.H.; grant no. MH126960: P.M.J.; grant no. R01 MH129751: S.J.S.), EMBO (ALTF 585-2021: C.A.), the Medical Research Council Centre of Research Excellence in Therapeutic Genomics (MR/Z504725/1: S.J.S., N.A.), the UCSF Bakar Aging Research Institute postdoctoral fellowship (C.A.) and the Bettencourt Schueller foundation (C.A.).

Author contributions Conceptualization: K.J.B., S.J.S., N.A. Methodology: S.T., A.D.N., P.W.E.S., H.K., J.Z., N.M., J.Q.P., J.T.P., P.M.J., R.B.-S., N.A., K.J.B. Software: H.K., J.Z., R.B.-S. Formal analysis: S.T., A.D.N., P.W.E.S., V.B., B.K., L.M., P.M.J., H.K., J.Z., K.J.B. Investigation: S.T., A.D.N., P.W.E.S., E.C.H., X.Z., H.K., Z.L., C.A., V.B., K.Y., J.Z., S.S.H., A.S., C.M.K., C.L., S.E.T., S.S., Y.C.L., K.J.B. Writing—original draft: S.T., A.D.N., N.A., K.J.B. Writing—review and editing: all authors. Visualization: S.T., A.D.N., P.W.E.S., H.K., J.Z., K.J.B. Supervision: N.A., K.J.B. Funding acquisition: S.T., A.D.N., P.W.E.S., S.S.H., J.Q.P., J.T.P., S.J.S., N.A., K.J.B.

Competing interests N.M. is the cofounder and former board member and CSO of Regel Therapeutics, N.A. is the cofounder of Regel Therapeutics and both N.A. and K.J.B. are on the scientific advisory board of Regel Therapeutics. P.W.E.S. is a Program Director at Regel Therapeutics. N.M. and N.A. are the inventors on patent 'Gene therapy for haploinsufficiency' WO2018148256A9. N.A., K.J.B. and S.J.S. receive funding from BioMarin Pharmaceutical Incorporated. The other authors declare no competing interests.

Additional information

Supplementary information The online version contains supplementary material available at https://doi.org/10.1038/s41586-025-09522-w.

Correspondence and requests for materials should be addressed to Nadav Ahituv or Kevin J. Bender.

Peer review information *Nature* thanks Elvir Becirovic, James Trimmer and the other, anonymous, reviewer(s) for their contribution to the peer review of this work. Peer reviewer reports are available.

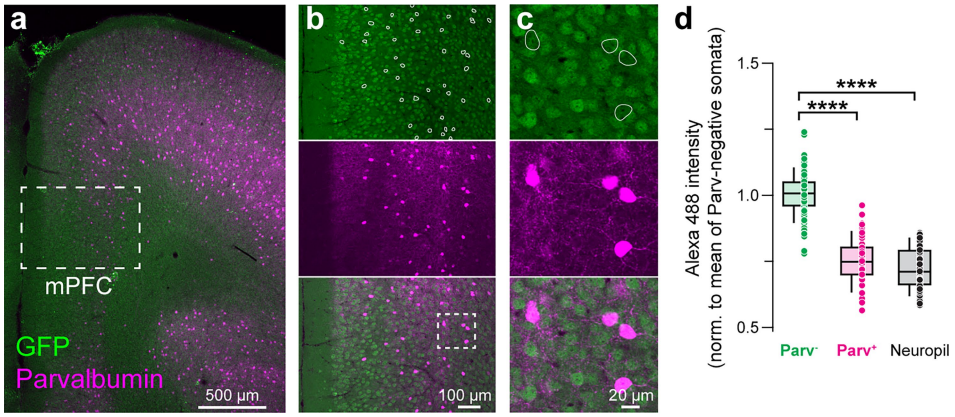

Extended Data Fig. 1 | Excitatory pyramidal neurons in the mPFC are GFP+ in Cre-negative *Scn2a*$^{+/KI}$ animals. a. Coronal brain sections from P60 *Scn2a*$^{+/KI}$ mouse (Cre-) immunostained with anti-GFP and anti-parvalbumin (PV). **b**. Zoom of area highlighted by dashed box in panel a, with GFP and Parvalbumin channels separated then merged at bottom. Parv+ somata are circled in the GFP panel. **c**. Further zoom of region in layer 5b in panel b. Parv+ somata are circled as in panel c. **d**. Quantification of mean fluorescence intensify of GFP in PV-negative cells, PV-positive cells, and neuropil (area without somata as a measure of background fluorescence). Data are from 2 mice. Circles are mean GFP intensity values in ROIs of Parv- somata, Parv+ somata, or neighboring neuropil in single optical sections. Box plots are medians, quartiles, and 100% tails. n = 67 Parv- and 37 Parv+ cells analyzed; Parv- vs. Parv + : ****$p < 0.0001$. Parv- vs. neuropil: ****$p < 0.0001$. Holm-Šídák multiple comparisons test.

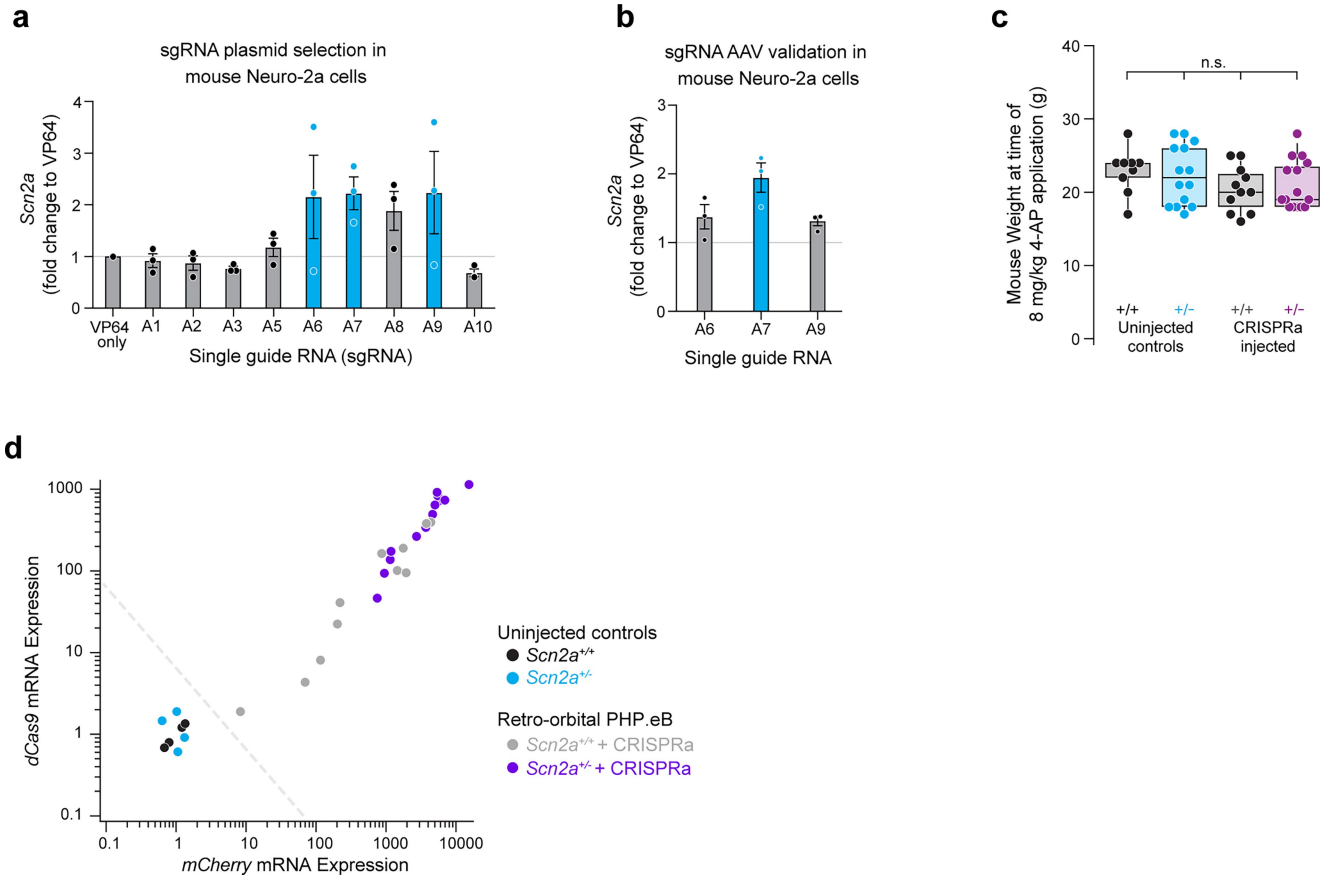

Extended Data Fig. 2 | In vitro optimization of CRISPRa constructs in mouse Neuroblastoma-2A cells. a. Fold change of *Scn2a* expression in Neuro-2a cells transfected with plasmids containing sgRNAs targeting the promoter of mouse *Scn2a* compared to a no-sgRNA VP64 control. Blue bars represent plasmids with largest increase in *Scn2a* expression. Circles are replicates, overlaid on mean ± SD. **b**. Fold change of *Scn2a* transduced with rAAV-DJ virus in Neuro-2a cells. Circles are replicates, overlaid on mean ± SD. **c**. Total animal weight at time of 8 mg/kg 4-AP administration (animals aged 69–119 days). Circles are animals. Box plots are medians, quartiles and 100% tails. **d**. RT-qPCR analysis of *dCas9* and *mCherry* mRNA within the mPFC of tail vein injected *Scn2a*$^{+/+}$ + CRISPRa (light gray) and *Scn2a*$^{+/-}$ + CRISPRa (purple) versus uninjected controls *Scn2a*$^{+/+}$ (dark gray) or Scn2a$^{+/-}$ (cyan). Injected animals with at least a 10-fold increase in expression levels of both dCas9 and *mCherry* to the average *Scn2a*$^{+/+}$ uninjected controls were included in EEG datasets in Fig. 3.

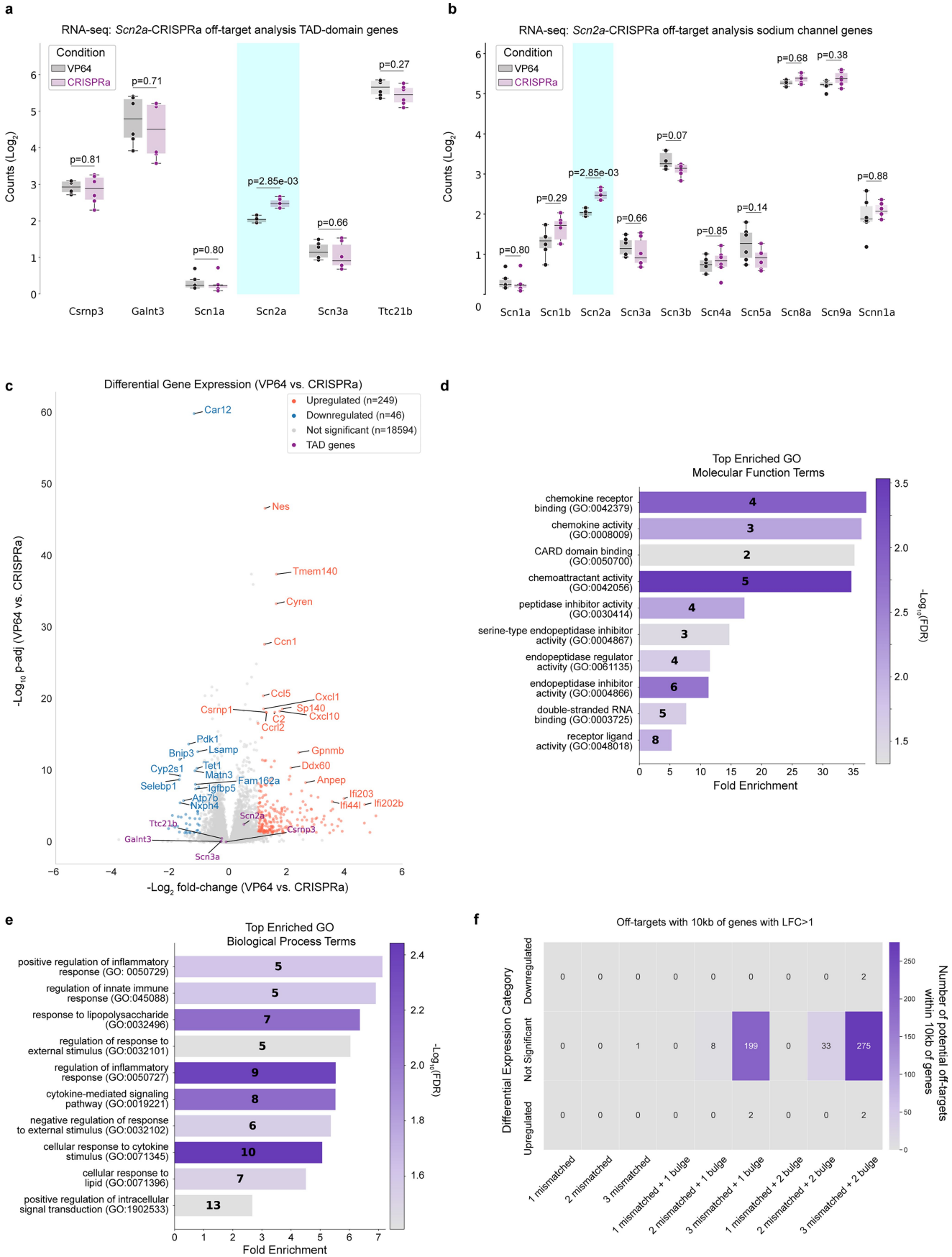

Extended Data Fig. 3 | See next page for caption.

Extended Data Fig. 3 | *Scn2a*-CRISPRa off-target analysis in cell lines. **a**. RNA-seq expression levels of *Scn2a* TAD-domain genes from *Scn2a*-rAAV-CRISPRa treated Neuro-2a cells compared to VP64-only. Circles are individual replicates, box plots are medians, quartiles and 100% tails. p-values noted above data. Wald test. **b**. RNA-seq expression levels of sodium channels from *Scn2a*-rAAV-CRISPRa treated Neuro-2a cells compared to VP64-only. Circles are individual replicates, box plots are medians, quartiles and 100% tails. p-values noted above data. Wald test. **c**. Volcano plot representing Log_2 fold-change in expression levels for each gene. Wald test. P-values noted above each comparison. Grey dots represent no significant DEGs for CRISPRa, purple dots signify *Scn2a* and nearby genes, and orange dots denote upregulated genes. **d**. Gene ontology (GO) analysis showing enrichment of molecular functions. **e**. Gene ontology (GO) analysis showing enrichment of biological processes. **f**. Analysis of sgRNA sequence off-targeting using Cas-OFFinder.

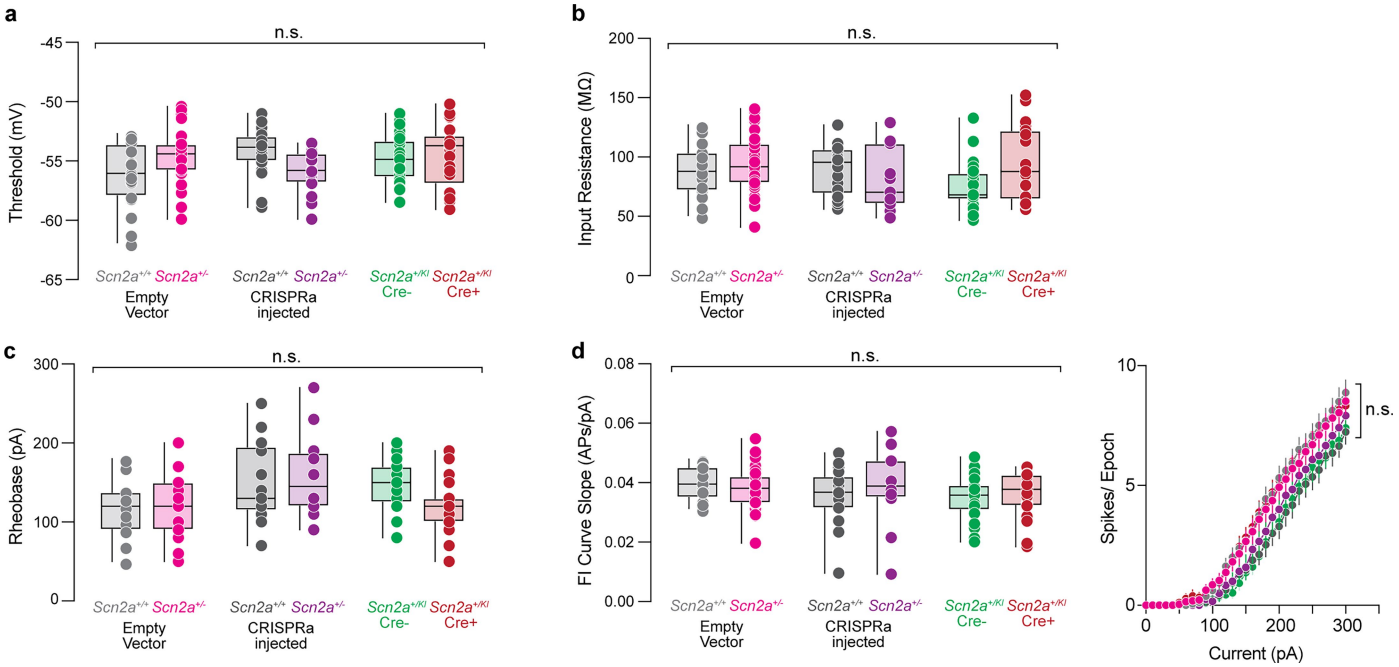

Extended Data Fig. 4 | Intrinsic electrophysiology of *Scn2a*$^{+/KI}$ and CRISPRa treated neurons. a. AP threshold from P57-85 *Scn2a*-rAAV-empty vector *Scn2a*$^{+/+}$ (light gray) and *Scn2a*$^{+/-}$ (magenta) neurons, *Scn2a*-rAAV-CRISPRa treated *Scn2a*$^{+/+}$ (dark gray) and *Scn2a*$^{+/-}$ (purple) neurons, and *Scn2a*$^{+/KI}$ Cre- (green) and *Scn2a*$^{+/KI}$ Cre+ (gray) neurons. Threshold of the first AP evoked by a near-rheobase current. *Scn2a*$^{+/+}$ + empty: n = 17 cells; *Scn2a*$^{+/-}$ + empty: n = 27 cells; *Scn2a*$^{+/+}$ + CRISPRa: n = 24 cells; *Scn2a*$^{+/-}$ + CRISPRa: n = 19 cells; *Scn2a*$^{+/KI}$ Cre-: n = 29 cells; *Scn2a*$^{+/KI}$ Cre + : n = 21 cells. No significant differences. Holm-Šídák multiple comparisons test. Circles are individual cells, box plots are medians, quartiles and 100% tails. **b**. Input resistance (MΩ). *Scn2a*$^{+/+}$ + empty: n = 17 cells; *Scn2a*$^{+/-}$ + empty: n = 27 cells; *Scn2a*$^{+/+}$ + CRISPRa: n = 17 cells; *Scn2a*$^{+/-}$ + CRISPRa: n = 11 cells; *Scn2a*$^{+/KI}$ Cre-: n = 26 cells; *Scn2a*$^{+/KI}$ Cre + : n = 19 cells. No significant differences. Holm-Šídák multiple comparisons test. Circles are individual cells, box plots are medians, quartiles and 100% tails. **c**. Rheobase current (pA) to generate first spike. *Scn2a*$^{+/+}$ + empty: n = 16 cells; *Scn2a*$^{+/-}$ + empty: n = 27 cells; *Scn2a*$^{+/+}$ + CRISPRa: n = 17 cells; *Scn2a*$^{+/-}$ + CRISPRa: n = 12 cells; *Scn2a*$^{+/KI}$ Cre-: n = 25 cells; *Scn2a*$^{+/KI}$ Cre + : n = 19 cells. No significant differences. Holm-Šídák multiple comparisons test. Circles are individual cells, box plots are medians, quartiles and 100% tails. **d**. APs per 300 ms stimulation epoch for each current amplitude. Left: Quantification of firing rate slope of data on Right. *Scn2a*$^{+/+}$ + empty: n = 16 cells; *Scn2a*$^{+/-}$ + empty: n = 27 cells; *Scn2a*$^{+/+}$ + CRISPRa: n = 17 cells; *Scn2a*$^{+/-}$ + CRISPRa: n = 12 cells; *Scn2a*$^{+/KI}$ Cre-: n = 25 cells; *Scn2a*$^{+/KI}$ Cre + : n = 19 cells. No significant differences. Holm-Šídák multiple comparisons test. Circles are individual cells, box plots are medians, quartiles and 100% tails.Right: Number of APs versus current amplitude injected. Circles and bars are mean ± SEM at each stimulus intensity.

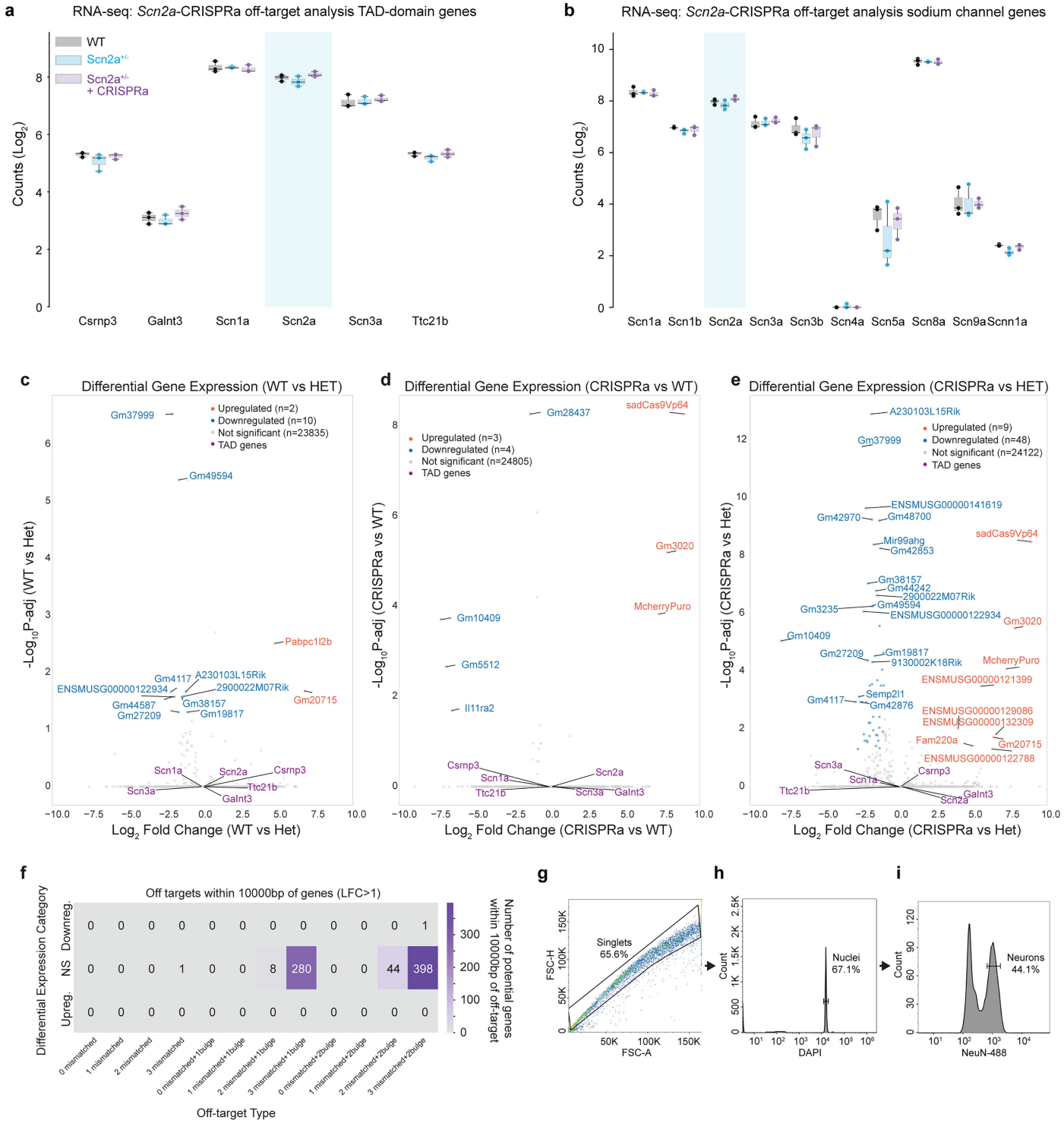

Extended Data Fig. 5 | *Scn2a*-CRISPRa off-target analysis in the mouse neocortex. a. RNA-seq expression levels of *Scn2a* TAD-domain genes from *Scn2a*-rAAV-CRISPRa treated Neuro-2a cells compared to VP64-only. Circles are individual mice, box plots are medians, quartiles and 100% tails. **b**. RNA-seq expression levels of sodium channels from *Scn2a*-rAAV-CRISPRa treated Neuro-2a cells compared to VP64-only. Circles are individual mice, box plots are medians, quartiles and 100% tails. **c**. Volcano plot representing Log_2 fold-change in expression levels for each gene for WT vs *Scn2a*$^{+/-}$ "Het". Wald test. P-values noted above each comparison. Grey dots represent no significant DEGs for CRISPRa, purple dots signify *Scn2a* and nearby genes, and orange dots denote upregulated genes. **d**. Same as c, but for CRISPRa-treated *Scn2a*$^{+/-}$ "CRISPRa" vs WT. **e**. Same as c, but for CRISPRa-treated *Scn2a*$^{+/-}$ "CRISPRa" vs *Scn2a*$^{+/-}$ "Het". **f**. Analysis of sgRNA sequence off-targeting using Cas-OFFinder. **g**. Data representation of NeuN-positive neuronal nuclei isolated from cortical tissue for FACS sorting. Representative FACS plots visualized with FlowJo V10 with percentage of parent gates for each population. Singlets were selected based on FSC-H versus FSC-A. **h**. From singlets, DAPI-positive events were gated to identify nuclei. **i**. NeuN-positive neuronal nuclei were selected using an anti-NeuN antibody conjugated to Alexa Fluor 488.

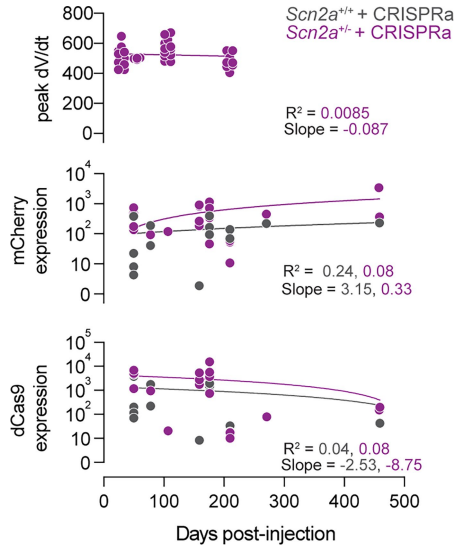

Extended Data Fig. 6 | CRISPRa expression persists through 16 months post-systemic injection. Peak AP dV/dt (top) at 30-, 56-, 107-, and 210-days following tail-vein injection of *Scn2a*-rAAV-CRISPRa-PHP.eB in *Scn2a*$^{+/-}$ mice (purple). Circles represent individual neurons. Lines are linear regression. qPCR of mCherry (middle) or dCas9 (bottom) mRNA from neocortical samples collected from tail-vein or retro-orbital *Scn2a*-rAAV-CRISPRa-PHP.eB injected *Scn2a*$^{+/+}$ (gray) or *Scn2a*$^{+/-}$ mice (purple) across time. Circles represent single mice. Lines are linear regression.

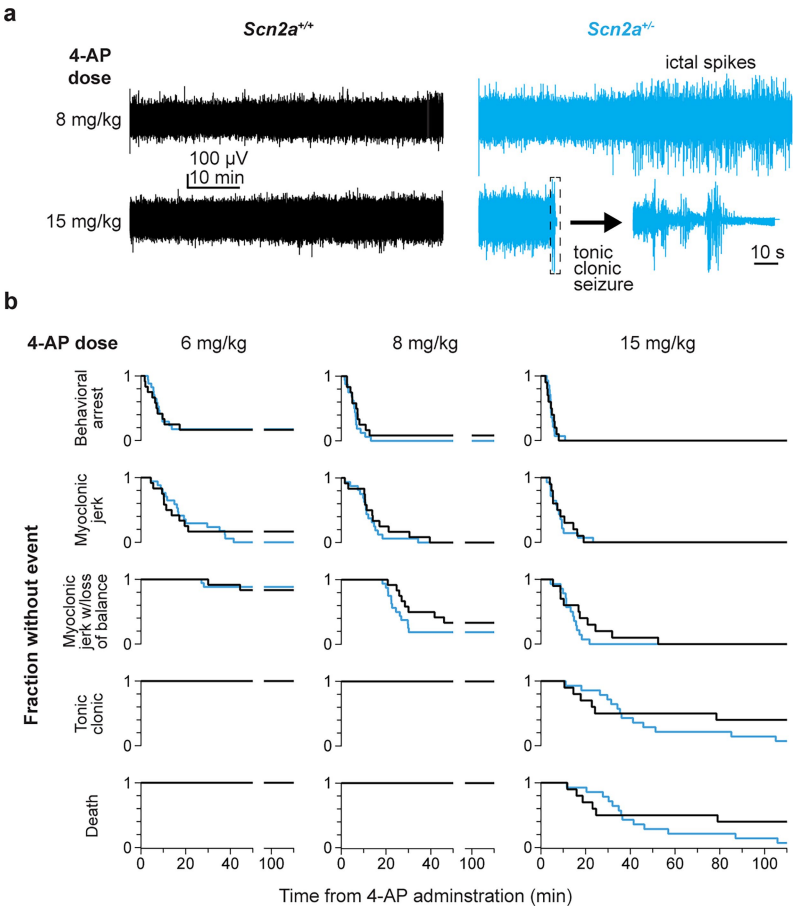

Extended Data Fig. 7 | Behavioral and EEG response to increasing doses of 4-AP in *Scn2a*$^{+/-}$ mice. a. Example PFC EEGs from animals receiving 8 and 15 mg/kg 4-AP. 4-AP administered at onset of all recordings. Dashed box denotes a tonic clonic seizure and subsequent mortality occurring with 15 mg/kg dosing in *Scn2a*$^{+/-}$ animal. EEG data within boxed area is shown at higher resolution on right. **b.** Survival curves for all WT and *Scn2a*$^{+/-}$ animals for 6, 8 and 15 mg/kg 4-AP. WT: black, *Scn2a*$^{+/-}$: cyan.

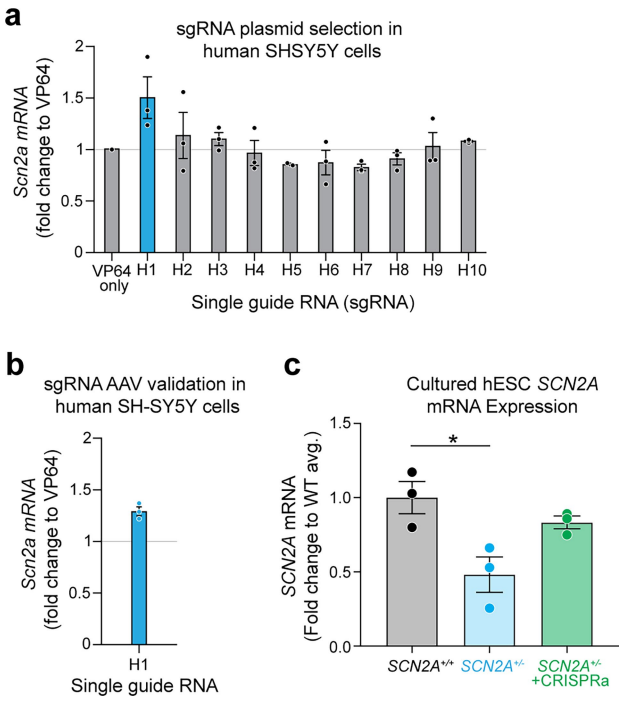

Extended Data Fig. 8 | In vitro optimization of CRISPRa constructs in human SH-SY5Ycells. a. Fold change of *SCN2A* expression in SH-SY5Y cells transfected with plasmids containing sgRNAs targeting the promoter of human *SCN2A* compared to a no sgRNA VP64 control. **b**. Fold change of *SCN2A* transduced with rAAV-DJ virus in human SH-SY5Y cells. **c**. *SCN2A* mRNA expression from *SCN2A*$^{+/+}$ (black), *SCN2A*$^{+/-}$ (cyan), and *SCN2A*-rAAV-CRISPRa treated *SCN2A*$^{+/-}$ (purple) hESC-derived neurons normalized to wild type average. *SCN2A*$^{+/+}$ vs. *SCN2A*$^{+/-}$: *p = 0.03. Holm-Šídák multiple comparisons test. n = 3 replicates for all conditions. circles are individual replicates. Bars are mean ± SD.

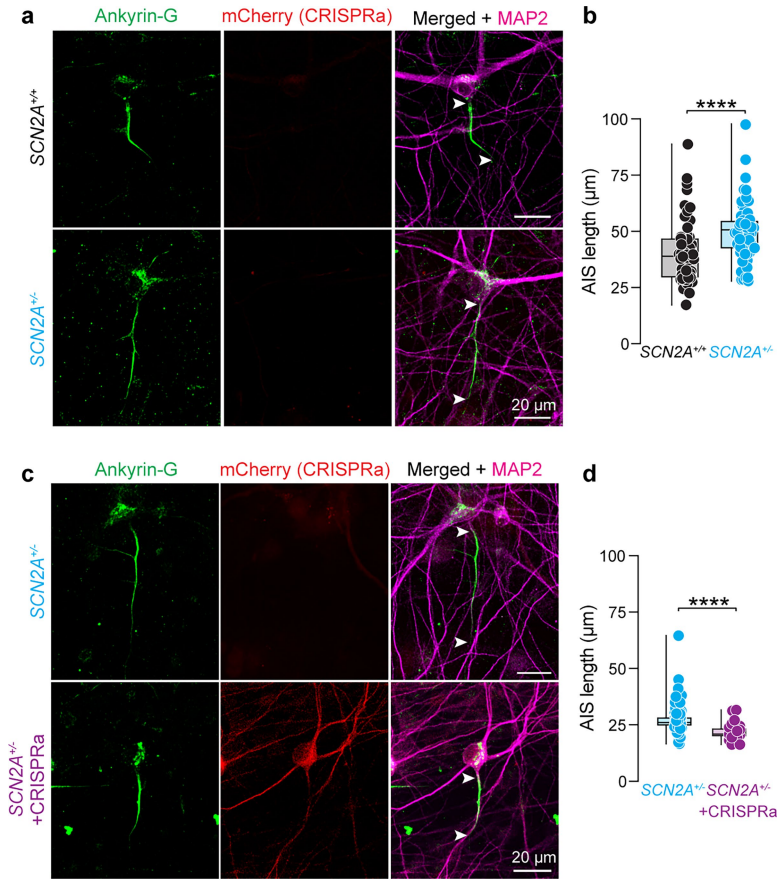

Extended Data Fig. 9 | Axon initial segment structural plasticity occurs in *SCN2A*$^{+/-}$ neurons and is rescued by CRISPRa. a. Representative images of *SCN2A*$^{+/+}$ (black) and *SCN2A*$^{+/-}$ (cyan) human stem-cell-derived neurons immunostained with antibodies against ankyrin-G (green) and MAP2 (magenta). Arrowheads denote start and end points used to quantify AIS length. **b**. Quantification of AIS length. *SCN2A*$^{+/+}$: n = 56 cells, 3 dishes. *SCN2A*$^{+/-}$: n = 56 cells, 3 dishes. ****p < 0.0001. Mann-Whitney test. **c**. Representative images of *SCN2A*$^{+/-}$ neurons expressing *Scn2a*-rAAV-CRISPRa-mCherry (purple) and mCherry-negative internal *SCN2A*$^{+/-}$ controls (cyan). Immunostaining against ankyrin-G and MAP2. **d**. Quantification of AIS length. *SCN2A*$^{+/-}$: n = 122 cells, 3 dishes. *SCN2A*$^{+/-}$ + CRISPRa: n = 23 cells, 3 dishes. ****p < 0.0001. Mann-Whitney test. Circles are individual AIS calculations. Box plots are medians, quartiles, and 100% tails.

nature portfolio

Corresponding author(s): Kevin Bender

Last updated by author(s): Apr 30, 2025

Reporting Summary

Nature Portfolio wishes to improve the reproducibility of the work that we publish. This form provides structure for consistency and transparency in reporting. For further information on Nature Portfolio policies, see our Editorial Policies and the Editorial Policy Checklist.

Statistics

For all statistical analyses, confirm that the following items are present in the figure legend, table legend, main text, or Methods section.

n/a	Confirmed
☐	☒ The exact sample size (*n*) for each experimental group/condition, given as a discrete number and unit of measurement
☐	☒ A statement on whether measurements were taken from distinct samples or whether the same sample was measured repeatedly
☐	☒ The statistical test(s) used AND whether they are one- or two-sided *Only common tests should be described solely by name; describe more complex techniques in the Methods section.*
☒	☐ A description of all covariates tested
☐	☒ A description of any assumptions or corrections, such as tests of normality and adjustment for multiple comparisons
☐	☒ A full description of the statistical parameters including central tendency (e.g. means) or other basic estimates (e.g. regression coefficient) AND variation (e.g. standard deviation) or associated estimates of uncertainty (e.g. confidence intervals)
☐	☒ For null hypothesis testing, the test statistic (e.g. *F*, *t*, *r*) with confidence intervals, effect sizes, degrees of freedom and *P* value noted *Give P values as exact values whenever suitable.*
☒	☐ For Bayesian analysis, information on the choice of priors and Markov chain Monte Carlo settings
☐	☒ For hierarchical and complex designs, identification of the appropriate level for tests and full reporting of outcomes
☒	☐ Estimates of effect sizes (e.g. Cohen's *d*, Pearson's *r*), indicating how they were calculated

Our web collection on statistics for biologists contains articles on many of the points above.

Software and code

Policy information about availability of computer code

Data collection	IgorPro v7, PrairieView v5, Pinnacle Sirenia v3,
Data analysis	Data analyzed in IgorPro v7, MATLAB, Prism, No custom code was developed for this article. For RNA-seq, sequencing reads were trimmed on the 3' ends of reads where the quality score was less than 20 using trim galore 0.6.10 through nf-core RNA-seq pipeline version 3.18. Sequences were mapped to mm39 with STAR 2.7.8a and counts were computed using featureCounts with gtf provided from Ensembl (Mus_musculus.GRCm39.113). Post-alignment, gene annotation was carried out using Ensembl Transcripts release 113. Differential expression was characterized using DESeq2 version 1.44 (2024-05-01) and R version 4.4. Gene Ontology (GO) over-representation analysis was carried out using GSEApy version 1.1.3.

For manuscripts utilizing custom algorithms or software that are central to the research but not yet described in published literature, software must be made available to editors and reviewers. We strongly encourage code deposition in a community repository (e.g. GitHub). See the Nature Portfolio guidelines for submitting code & software for further information.

Data

Policy information about availability of data

All manuscripts must include a data availability statement. This statement should provide the following information, where applicable:

- Accession codes, unique identifiers, or web links for publicly available datasets
- A description of any restrictions on data availability
- For clinical datasets or third party data, please ensure that the statement adheres to our policy

All RNA-seq data is available on the NCBI Gene Expression Omnibus as Bioproject GSE193605. Source data for all statistical analyses are provided with this article. Requests for materials can be directed to NA (CRT-based approaches) or KJB (mouse models).

Research involving human participants, their data, or biological material

Policy information about studies with human participants or human data. See also policy information about sex, gender (identity/presentation), and sexual orientation and race, ethnicity and racism.

Reporting on sex and gender	N/A
Reporting on race, ethnicity, or other socially relevant groupings	N/A
Population characteristics	N/A
Recruitment	N/A
Ethics oversight	N/A

Note that full information on the approval of the study protocol must also be provided in the manuscript.

Field-specific reporting

Please select the one below that is the best fit for your research. If you are not sure, read the appropriate sections before making your selection.

☒ Life sciences ☐ Behavioural & social sciences ☐ Ecological, evolutionary & environmental sciences

For a reference copy of the document with all sections, see nature.com/documents/nr-reporting-summary-flat.pdf

Life sciences study design

All studies must disclose on these points even when the disclosure is negative.

Sample size	Group sample sizes were chosen based on standards in the field and previous similar experiments conducted by our group (e.g., Spratt et al., 2019). No statistical methods were used to predetermine sample size.
Data exclusions	Data exclusions were made solely for EEG analysis based on SCN2A, dCas and mCherry expression levels. Two of 23 animals were excluded due to a lack of upregulation, presumably due to failed injections.
Replication	All experiments were replicated in at least 3 animals, with multiple recordings from individual cells within animals. There were no failures of replication.
Randomization	All animals were allocated randomly into experimental groups.
Blinding	All experiments were performed blind to genotype.

Reporting for specific materials, systems and methods

We require information from authors about some types of materials, experimental systems and methods used in many studies. Here, indicate whether each material, system or method listed is relevant to your study. If you are not sure if a list item applies to your research, read the appropriate section before selecting a response.

Materials & experimental systems

n/a	Involved in the study
☐	☒ Antibodies
☐	☒ Eukaryotic cell lines
☒	☐ Palaeontology and archaeology
☐	☒ Animals and other organisms
☒	☐ Clinical data
☒	☐ Dual use research of concern
☒	☐ Plants

Methods

n/a	Involved in the study
☒	☐ ChIP-seq
☐	☒ Flow cytometry
☒	☐ MRI-based neuroimaging

Antibodies

Antibodies used: GFP, Parv, mCherry, Ank-G, MAP2

Validation:

GFP - anti-GFP AlexaFluor 488, ThermoFisher A-21311; Species reactivity: Mouse, Tag; Applications: ICC, IHC, WB, ChIP assay, Flow cytometry; Validation: https://www.thermofisher.com/antibody/product/GFP-Antibody-Polyclonal/A-21311

Parvalbumin - Swant P27; Species reactivity: Human, Rat, Mouse, Bovine and Equine; Applications: ICC, IHC, WB, IP, Flow cytometry, ELISA; Validation: https://webshop.swant.com/catalog/product/view/id/99/s/pv27a-parvalbumin/category/2/

mCherry - anti-RFP Rockland Immuno #600-401-379 ; Species reactivity: Rabbit; Applications: WB, ELISA, IHC, IF, EM, FISH, IP; Validation: https://www.rockland.com/categories/primary-antibodies/rfp-antibody-pre-adsorbed-600-401-379/

Ankyrin-G - Neuromab 75-146; Species reactivity: Feline, Hamster, Human, Mouse, Non-Human Primate, Rat; Applications: ICC, IHC, IP, WB; Validation: https://www.antibodiesinc.com/products/anti-ankyrin-g-staining-antibody-n106-36-75-146

MAP2 - Invitrogen PA1-10005; Species reactivity: Human, Mouse, Rat; Applications: ICC, IHC, WB, PLA; https:// Validation: www.thermofisher.com/antibody/product/MAP2-Antibody-Polyclonal/PA1-10005

Eukaryotic cell lines

Policy information about cell lines and Sex and Gender in Research

Cell line source(s): Neuro-2A and SH-SY5Y cells were obtained from ATCC. HUES66 wild type and SCN2A heterozygous iPSCs were obtained from Jen Q. Pan at the Stanley Center for Psychiatric Research, Broad Institute of MIT and Harvard.

Authentication: Neuro-2A and SH-SY5Y were ordered from ATCC. For the SCN2A HUES66 lines, these lines were extensively characterized in PMID 30698461.

Mycoplasma contamination: All lines were tested monthly for mycoplasma.

Commonly misidentified lines (See ICLAC register): N/A

Animals and other research organisms

Policy information about studies involving animals; ARRIVE guidelines recommended for reporting animal research, and Sex and Gender in Research

Laboratory animals: C57BL/6J mice, aged postnatal day 25 to 240. Mice are housed on a 12/12 hr light dark cycle, with ambient temperature maintained between 67-74° F and ambient humidity maintained between 30-70%.

Wild animals: No wild animals were used.

Reporting on sex: Data were collected from animals of both sexes. Prior work indicated that effects of Scn2a haploinsufficiency in mouse are not dependent on sex in the neuronal classes studied (Spratt et al., 2019). Therefore, data were pooled across sex.

Field-collected samples: No field collected samples were used.

Ethics oversight: UCSF Institutional Animal Care and Use Committee

Note that full information on the approval of the study protocol must also be provided in the manuscript.

Plants

Seed stocks — *Report on the source of all seed stocks or other plant material used. If applicable, state the seed stock centre and catalogue number. If plant specimens were collected from the field, describe the collection location, date and sampling procedures.*

Novel plant genotypes — *Describe the methods by which all novel plant genotypes were produced. This includes those generated by transgenic approaches, gene editing, chemical/radiation-based mutagenesis and hybridization. For transgenic lines, describe the transformation method, the number of independent lines analyzed and the generation upon which experiments were performed. For gene-edited lines, describe the editor used, the endogenous sequence targeted for editing, the targeting guide RNA sequence (if applicable) and how the editor was applied.*

Authentication — *Describe any authentication procedures for each seed stock used or novel genotype generated. Describe any experiments used to assess the effect of a mutation and, where applicable, how potential secondary effects (e.g. second site T-DNA insertions, mosiacism, off-target gene editing) were examined.*

Flow Cytometry

Plots

Confirm that:

☒ The axis labels state the marker and fluorochrome used (e.g. CD4-FITC).

☒ The axis scales are clearly visible. Include numbers along axes only for bottom left plot of group (a 'group' is an analysis of identical markers).

☒ All plots are contour plots with outliers or pseudocolor plots.

☒ A numerical value for number of cells or percentage (with statistics) is provided.

Methodology

Sample preparation — Mice cortices were dissected and nuclei were isolated from approximately 200 mg of cortex using the Singulator™ 100 System (S2 Genomics) with the "Single Shot Standard Nuclei Isolation v2" program. The isolation was performed in 3 mL of lysis buffer (10 mM Tris-HCl, pH 7.4; 10 mM NaCl; 3 mM $MgCl_2 \cdot 6H_2O$; 0.05% IGEPAL® CA-630; 0.5 mM DTT; nuclease-free water) and 3 mL of wash buffer (5% bovine serum albumin, 0.25% glycerol in 1× PBS). To preserve RNA integrity, 50 µL of Protector RNase Inhibitor (Sigma-Aldrich, #3335402001) was added directly to the Singulator cartridge. Following isolation, nuclei were centrifuged, and debris were removed by centrifugation in wash buffer supplemented with 1× Nuclei Debris Removal Stock Reagent (S2 genomics #100253628) and 37.5 µL of RNase inhibitor at 600 × g for 15 min at 4°C, with deceleration set to 1. Purified nuclei were then washed once in wash buffer and resuspended in 500 µL of wash buffer supplemented with 6.5 µL of Protector RNase Inhibitor, DAPI (Biotium, #40043; 1:1000), and anti NeuN-488 antibody (Sigma-Aldrich, #MAB377X; 1:500). The suspension was incubated for 1 hour at 4°C in the dark to allow staining. Finally, nuclei were washed once with wash buffer, resuspended in 1 mL of wash buffer supplemented with 12.5 µL of Protector RNase Inhibitor, and transferred to a FACS tube.

Instrument — BD FACS ARIA

Software — FACSDiva Software

Cell population abundance — The proportion of neuronal (NeuN-positive) nuclei among total nuclei was approximately 40%, depending on the sample and the enrichment of neuronal nuclei was evaluated post sorting by RNA-seq.

Gating strategy — Singlets were identified on the FSC-A versus FSC-H plot. Nuclei were gated as DAPI-positive events. Neuronal nuclei were then selected as NeuN-488–positive events.

☒ Tick this box to confirm that a figure exemplifying the gating strategy is provided in the Supplementary Information.